






Article

Molecular and Polymer Ln₂M₂ (Ln = Eu, Gd, Tb, Dy; M = Zn, Cd) Complexes with Pentafluorobenzoate Anions: The Role of Temperature and Stacking Effects in the Structure; Magnetic and Luminescent Properties

Maxim A. Shmelev ¹, Mikhail A. Kiskin ^{1,*}, Julia K. Voronina ¹,
Konstantin A. Babeshkin ¹, Nikolay N. Efimov ¹, Evgenia A. Varaksina ²,
Vladislav M. Korshunov ^{2,3}, Ilya V. Taydakov ^{2,4}, Natalia V. Gogoleva ¹, Alexey A. Sidorov ¹
and Igor L. Eremenko ¹

¹ N. S. Kurnakov Institute of General and Inorganic Chemistry, Russian Academy of Sciences, 119991 Moscow, Russia; shmelevma@yandex.ru (M.A.S.); juliavoronina@mail.ru (J.K.V.); bkonstantan@yandex.ru (K.A.B.); nnefimov@yandex.ru (N.N.E.); judiz@rambler.ru (N.V.G.); sidorov@igic.ras.ru (A.A.S.); ilerem@igic.ras.ru (I.L.E.)

² P. N. Lebedev Physical Institute, Russian Academy of Sciences, 119991 Moscow, Russia; janiy92@yandex.ru (E.A.V.); vladkorshunov@bk.ru (V.M.K.); taidakov@mail.ru (I.V.T.)

³ Faculty of Fundamental Sciences, Bauman Moscow State Technical University, 105005 Moscow, Russia

⁴ Academic Department of Innovational Materials and Technologies Chemistry, Plekhanov Russian University of Economics, 117997 Moscow, Russia

* Correspondence: mkiskin@igic.ras.ru

Received: 12 November 2020; Accepted: 8 December 2020; Published: 13 December 2020



Abstract: Varying the temperature of the reaction of $[\text{Cd}(\text{pfb})(\text{H}_2\text{O})_4]^{+n} \cdot n(\text{pfb})^{-}$, $[\text{Ln}_2(\text{pfb})_6(\text{H}_2\text{O})_8] \cdot \text{H}_2\text{O}$ (Hpfb = pentafluorobenzoic acid), and 1,10-phenanthroline (phen) in MeCN followed by crystallization resulted in the isolation of two type of products: 1D-polymers $[\text{LnCd}(\text{pfb})_5(\text{phen})]_n \cdot 1.5n\text{MeCN}$ (Ln = Eu (I), Gd (II), Tb (III), Dy (IV)) which were isolated at 25 °C, and molecular compounds $[\text{Tb}_2\text{Cd}_2(\text{pfb})_{10}(\text{phen})_2]$ (V) formed at 75 °C. The transition from a molecular to a polymer structure becomes possible because of intra- and intermolecular interactions between the aromatic cycles of phen and pfb from neighboring tetranuclear Ln₂Cd₂ fragments. Replacement of cadmium with zinc in the reaction resulted in molecular compounds Ln₂Zn₂ $[\text{Ln}_2\text{Zn}_2(\text{pfb})_{10}(\text{phen})_2] \cdot 4\text{MeCN}$ (Ln = Eu (VI), Tb (VIII), Dy (IX)) and $[\text{Gd}_2\text{Zn}_2(\text{pfb})_{10}(\text{H}_2\text{O})_2(\text{phen})_2] \cdot 4\text{MeCN}$ (VII). A new molecular EuCd complex $[\text{Eu}_2\text{Cd}_2(\text{pfb})_{10}(\text{phen})_4] \cdot 4\text{MeCN}$ (X) was isolated from a mixture of cadmium, zinc, and europium pentafluorobenzoates (Cd:Zn:Ln = 1:1:2). Complexes II-IV, VII and IX exhibit magnetic relaxation at liquid helium temperatures in nonzero magnetic fields. Luminescent studies revealed a bright luminescence of complexes with europium(III) and terbium(III) ions.

Keywords: cadmium-lanthanide(III) complexes; zinc-lanthanide(III) complexes; pentafluorobenzoic acid; coordination polymer; single crystal X-ray; magnetochemistry; photoluminescence

1. Introduction

Luminescent lanthanide complexes attracted much attention because of their potential applications in biomedical imaging, catalysis [1], quantum computing technics [2], magnetic refrigerators [3], sorbents [4], luminescent sensors, and fluorescent probes [5]. The narrow bandwidth of the f-f transitions, the long luminescence lifetime (~ms) and the presence of high magnetic anisotropy determine the interest in the studies being carried out and the prospects for practical applications.

The use of aromatic ligands in the design of complexes of luminescent lanthanides is required to enhance their emission. Carboxylate ligands were studied as efficient sensitizers for luminescent lanthanide complexes as well as molecular magnets [6,7]. Fluorinated organic ligands are actively used to improve the intensity of luminescence of complexes by reducing the effect of fluorescence quenching by the vibrational C-H bond [8–12]. For example, Eu(III) perfluorobenzoates reveal much higher luminescence than benzoates [13]. Terbium(III) and europium(III) fluorobenzoates were shown to possess high luminescence intensity with quantum yields up to 70% [14]. The use of co-ligands and/or d-metals in the design of lanthanide complexes leads to structural modification needed to improve their luminescent and/or magnetic properties due to additional antenna effect, control the geometry of the coordination polyhedra of lanthanide atoms, minimize interionic interactions, etc. [15–22]. Fluorinated polycarboxylic acids are used for the synthesis of coordination polymers (CPs) as well as metal organic frameworks (MOFs). Fluorinated lanthanide MOFs/CPs are of great interest for their applications as OLED (organic light-emitting diode) sensors, in biomedical analysis and in cell imaging [12,14,23–26].

A special role in the formation of complexes with anions of fluorinated carboxylic acids and aromatic N-donor ligands is played by π - π interactions between the aromatic fragments of heteroligands, which additionally stabilize the crystal structure [27–29]. Additionally, fluorinated carboxylic acids are involved in the formation of C-H...F and C...F, F...F contacts, which also affect the stability of the crystal packing of the complexes [5,30–32]. These intra- and intermolecular interactions can positively affect the luminescent properties of the resulting complexes [33–35].

This work presents the results on the synthesis of LnZn and LnCd complexes with pentafluorobenzoate anions (Hpfb) and 1,10-phenantrolin (phen) molecules. In spite of the fact that studies of heterometallic complexes are attracting more and more attention in the search for ways to modify physicochemical properties, this area of coordination chemistry remains scarcely studied. A series of hitherto unknown molecular and polymeric LnZn and LnCd complexes were obtained and the conditions for the conversion of the molecular form of a LnCd complex to the corresponding 1D polymeric one without changing the compound composition were determined. The magnetic and luminescent properties were compared systematically.

2. Results

2.1. Synthesis of Complexes

The reaction between $[\text{Cd}(\text{pfb})(\text{H}_2\text{O})_4]^{+n} \cdot n(\text{pfb})^{-}$ [28] and $[\text{Ln}_2(\text{pfb})_6(\text{H}_2\text{O})_8] \cdot 2\text{H}_2\text{O}$ [13,36] in the presence of phen (in the 2:1: 2 ratio, respectively) in MeCN at room temperature gave a series of 1D-coordination polymers with the composition $[\text{LnCd}(\text{pfb})_5(\text{phen})]_n \cdot 1.5n\text{MeCN}$ (Ln = Eu (I), Gd (II), Tb (III), Dy (IV)) (yield ~65–80%). It was found that increasing the synthesis temperature to 75 °C and crystallization of III in a sealed vial allowed us to isolate the crystals of $[\text{Tb}_2\text{Cd}_2(\text{pfb})_{10}(\text{phen})_2]$ (V) complex in ~40% yield. The composition of V is similar to that of polymer III, except for the presence or absence of solvate molecules. Compound V is a molecular complex, as confirmed by X-ray diffraction data. Isolation of molecular complexes with Eu^{3+} , Gd^{3+} , and Dy^{3+} cations was delayed by a search for the temperature conditions for reproducible isolation of single crystals as single-phase products.

On replacement of the cadmium salt with the zinc one in reactions for the synthesis of I–V and at the synthesis and crystallization temperatures varied from 25 °C to 80 °C, only tetranuclear complexes with the composition $[\text{Ln}_2\text{Zn}_2(\text{pfb})_{10}(\text{phen})_2] \cdot 4\text{MeCN}$ (Ln = Eu (VI), Tb (VIII), Dy (IX)) and $[\text{Gd}_2\text{Zn}_2(\text{pfb})_{10}(\text{H}_2\text{O})_2(\text{phen})_2] \cdot 4\text{MeCN}$ (VII) were precipitated in a good yield (60–80%).

Our attempt to synthesize a heterometallic {LnZnCd} compound using the above reagents in the ratio Zn: Cd: Eu: phen = 1:1:1:2 resulted in the crystallization of a new molecular EuCd heterometallic complex $[\text{Eu}_2\text{Cd}_2(\text{pfb})_{10}(\text{phen})_4] \cdot 4\text{MeCN}$ (X) in about 20% yield.

The resulting compounds were obtained as single-crystal and polycrystalline solids. The purity of the bulky obtained samples was proven by PXRD (see supporting information, Figures S1–S9). All the

new compounds were characterized by C, H, N-analysis and IR spectroscopy. The equivalence of their compositions with the molecular formulas was confirmed by X-ray diffraction studies.

Isostructural compounds I–IV were crystallized as single-crystal solvates with acetonitrile; they were found to consist of polymer chains of alternating pairs of Cd and Ln atoms, which form tetranuclear Ln_2Cd_2 fragments (Figure 1). The chain growth occurs via bridging and chelate-bridging carboxylate anions. The coordination polyhedron LnO_9 is a muffin constructed by oxygen atoms of three bridging, three chelate-bridging, and one bidentate-coordinated carboxylate anions (Tables 1 and S1). The coordination polyhedron CdO_5N_2 is a pentagonal bipyramid formed by three chelate-bridging and one bridging carboxylate anion and completed by the coordination of two nitrogen atoms of the phenanthroline molecule (Tables 1 and S1). The elementary chain unit is a fragment that contains one Cd atom and one Ln atom; the chain growths occurs through the center of inversion. As a result, a metal core is formed in which the cadmium and lanthanum atoms are located in different planes. The angle between these planes is about 80° , and the aromatic fragments of the ligands are arranged symmetrically in opposite quarters formed by the intersection of these planes. The aromatic nature of all substituents and their almost strictly perpendicular arrangement results in a significant amount of $\pi\cdots\pi$ overlaps throughout the polymer chain. The geometric parameters of these interactions (the distances between the planes of the cycles are 3.2–3.4 Å, the angles between these planes are $4\text{--}6^\circ$, Table S2) indicate that they have high strength and make a large contribution to the formation of the structure of the polymers studied because of there are very many of them.

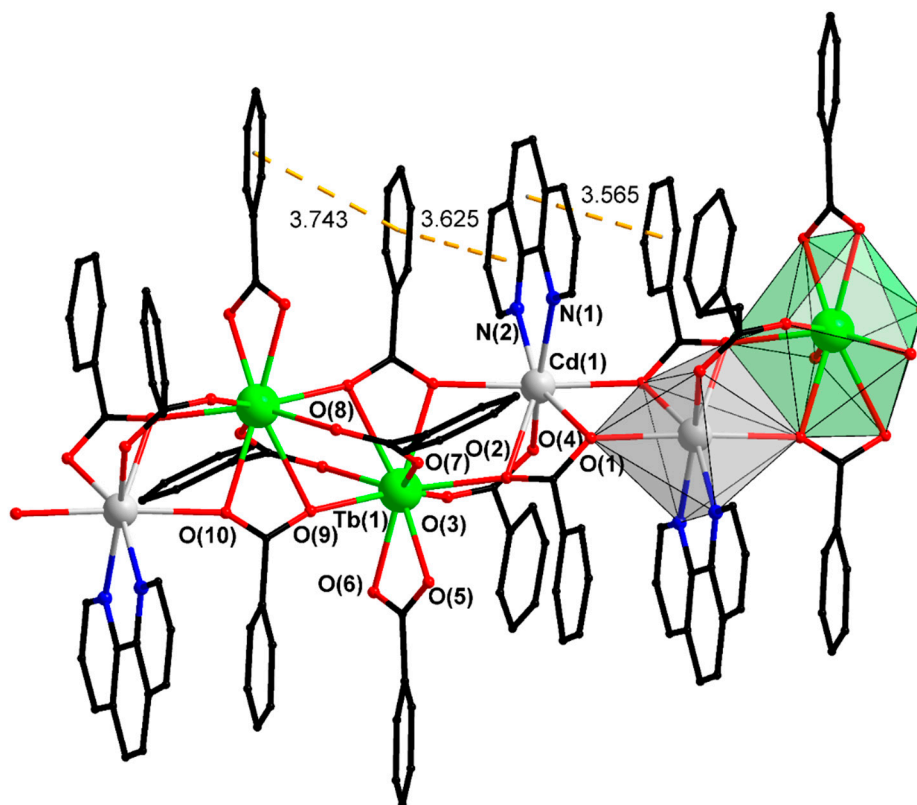


Figure 1. A fragment of polymeric chain of III. Hydrogen and fluorine atoms are omitted (dotted lines).

Table 1. Selected bond lengths, the shortest interatomic distances d (Å) and angles ω (°) in structures I–V, X.

Compound/Parameter	I	II	III	IV	V	X
Bond Lengths	d (Å)					
Cd–O (pfb)	2.207(4)– 2.468(5)	2.206(5)– 2.480(5)	2.215(4)– 2.469(4)	2.212(5)– 2.485(6)	2.252(3)– 2.405(3)	2.210(8)– 2.457(10)
Cd–N (phen)	2.314(5), 2.320(5)	2.304(5), 2.317(5)	2.319(5), 2.324(5)	2.262(15)– 2.44(2)	2.290(3), 2.345(3)	2.264(10), 2.320(11)
Ln–O (pfb)	2.370(3)– 2.728(4)	2.364(4)– 2.719(4)	2.350(4)– 2.729(4)	2.329(4)– 2.734(4)	2.314(3)– 2.655(3)	2.325(7)– 2.442(7)
Ln–N (phen)	-	-	-	-	-	2.602(9), 2.636(9)
Interatomic distances	d (Å)					
Cd ... Ln	3.987(1)	3.971(2)	3.974(1)	3.964(1)	3.917(1)	4.453(1)
Ln ... Ln	4.178(1)	4.173(2)	4.164(1)	4.153(1)	4.015(1)	4.408(1)
Cd ... Cd	3.923(1)	3.948(2)	3.926(4)	3.940(1)	7.793(1)	6.782(19)
Bond angles	ω (°)					
Cd–Ln–Ln	115.25(3)	115.57(5)	115.23(3)	115.39(2)	171.62(1)	162.57(3)

The polymer chains in the crystal are located parallel to the crystallographic axis a and are bonded by C–F ... π and C–H ... F interactions (Table S3). The acetonitrile molecules are embedded in the crystal lattice due to C–H...N and C–N... π interactions (Table S4).

Compound V is a molecular tetranuclear complex consisting of two Ln atoms in the center of the molecule and two cadmium atoms on the periphery (Figure 2). The chemical composition of the complex is identical to that of polymer III; therefore, it is of particular interest to compare the structures of molecular complex V and the analogous tetranuclear fragment in III. The metal atoms in compound V are in the same plane, which results in an increase in the Cd–Tb–Tb angle (115.23(3)° and 171.62(1)° in III and V, respectively) and the distance between the cadmium atoms in comparison with compound III (10.463(4) Å in III and 11.822(1) Å in V). The coordination polyhedron TbO₈ is a triangular dodecahedron. The geometry of the CdO₅N₂ polyhedron is a pentagonal bipyramid (Table S1). A detailed analysis of the geometric parameters and the overlap of the corresponding fragments showed that the central fragment of two lanthanides bound by pentafluorobenzoic anions is identical in the structures of III and V; the polymer and molecular complexes differ by the structures of the Ln–Cd fragments. This is due to the mutual arrangement of the aromatic fragments of the ligands. In V, the C₆F₅ fragments are located quite freely and the intramolecular π ... π overlaps are weak (Table S2); the phenanthroline molecules “close” the complex and are located practically perpendicular to the planes of the C₆F₅ rings. The large aromatic fragments of phen of neighboring molecules in a crystal of V overlap each other, participating in a strong π ... π interaction and forming the main supramolecular motif of the crystal structure of this compound—infinite chains located along the main diagonal of the crystal (Table S2). Due to C–F... π , C–H ... O, and C–H...F interactions, the chains are stacked parallel to each other to form a three-dimensional crystal structure (Table S4).

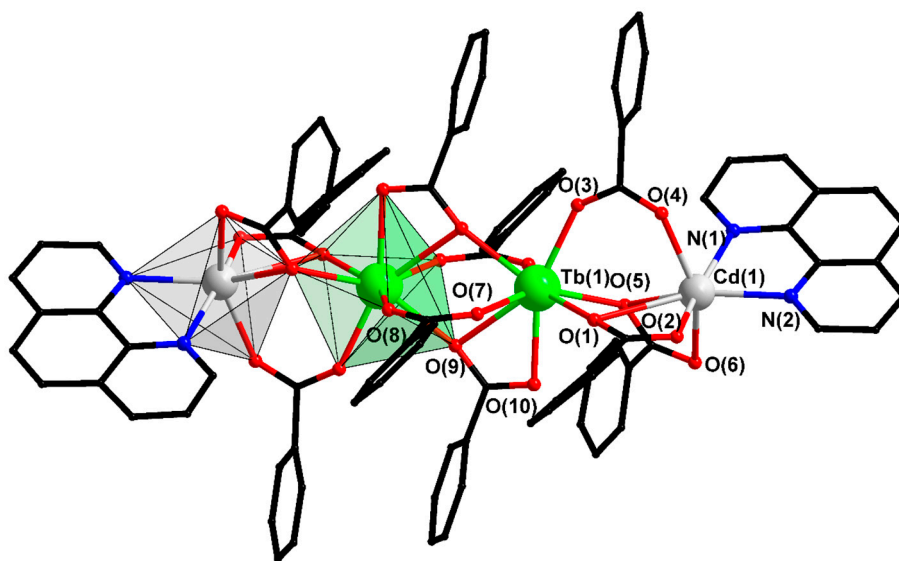


Figure 2. Structure of complex V. Hydrogen and fluorine atoms are omitted.

Compounds VI–IX are zinc analogs of molecular complex V. The geometry of the “central” lanthanide fragment in them is the same as in V (Figure 3). In addition, the geometry of the Ln–Zn fragment slightly differs due to a change in the type of binding of pfb-anions. First of all, the changes in the structure of the complexes appear in lanthanide polyhedra: in isostructural compounds VI, VIII, and IX, three different polyhedrons have the same coordination number equal to that in VIII, while in the structure of VII there is an additional coordinated water molecule; as a result, the changes are most significant (Tables 2 and S1). The heterometallic atoms in VI–IX are bound by one chelate-bridging and two bridging pfb-groups (the geometry of the ZnO_6N_2 polyhedron corresponds to a distorted octahedron (Table S1)); as a result, there is a redistribution of longer and shorter bonds, which results in a change in the relative positions of the C_6F_5 rings and $\pi\cdots\pi$ interactions involving these rings (Table S2).

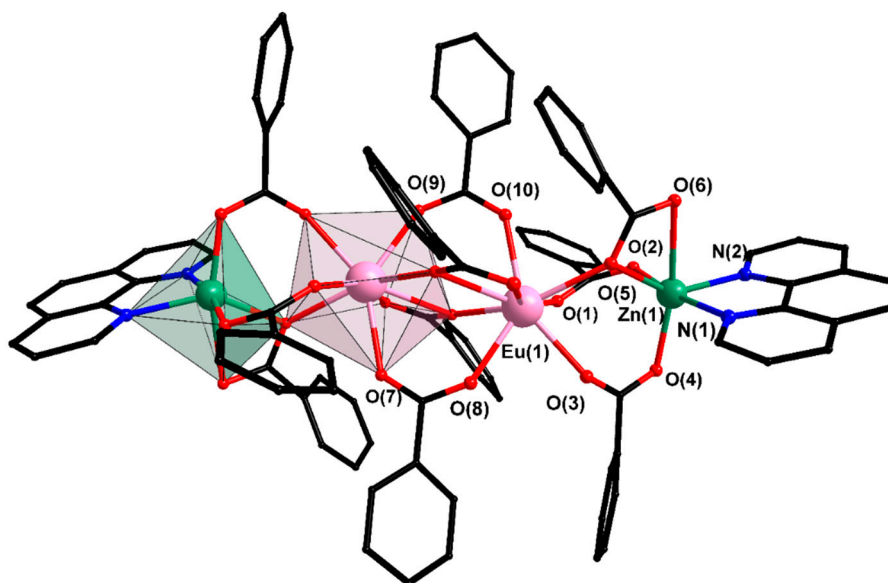


Figure 3. Structure of complex VI. Hydrogen and fluorine atoms are omitted.

Table 2. Selected bond lengths, the shortest interatomic distances d (Å) and angles ω (°) in structures VI–IX.

Compound/Parameter	VI	VII	VIII	IX
Bond Lengths	d (Å)			
Zn–O (pfb)	2.037(4)–2.454(5)	2.037(2)–2.357(2)	2.037(3)–2.436(3)	2.028(3)–2.452(3)
Zn–N (phen)	2.088(5), 2.137(5)	2.108(3), 2.135(2)	2.091(3), 2.137(4)	2.088(3), 2.135(3)
Ln–O (pfb)	2.340(4)–2.608(4)	2.357(2)–2.572(2)	2.317(3)–2.607(3)	2.291(2)–2.576(2)
Ln–O (H ₂ O)	-	2.426(2)	-	-
Interatomic distances	d (Å)			
Zn ... Ln	3.857(1)	3.392(1)	3.864(1)	3.819(1)
Ln ... Ln	3.986(1)	3.991(1)	3.965(1)	3.917(1)
Zn ... Zn	7.783(1)	7.936(1)	7.828(1)	7.946(1)
Bond angles	ω (°)			
Zn–Ln–Ln	161.77	160.30	162.12	162.17

In addition, the phenanthroline fragments of neighboring molecules in the crystals of these compounds are located slightly more closely than in cadmium complexes, which indicates a slightly higher energy of their overlapping. In general, the crystal structure of zinc complexes is similar to that of cadmium complexes, i.e., parallel chains of molecules linked by weak interactions into a three-dimensional lattice.

The structure of complex VII differs from those of VI, VIII, and IX. It has an additional water molecule coordinated by the gadolinium atom. This leads both to a change in the polyhedron of the corresponding atom (capped square antiprism) and to changes in the structure of the complex (Table S1). The Ln–Ln distances are slightly elongated while the Zn–Ln distances are shortened (Table 2). The appearance of a hydrogen bonding center—a water molecule—in the structure of VII promotes H-bonding of MeCN solvate molecules via classical H-bonds (Table S3).

The packing of crystals VI–IX is realized due to $\pi\cdots\pi$, C–F $\cdots\pi$, C–H \cdots O and C–H \cdots F interactions (Tables S2–S4).

Compound X (Figure 4, Table 1) is a molecular complex similar to V. The difference is that the place of one pfb-ligand is occupied by an additional phenanthroline molecule coordinated by the Eu1 atom. The carboxylate anions change their character from chelate-bridging to bridging in the central Eu2 fragment, thereby freeing up one coordination place on the Eu1 atom, while the chelate-bridging pfb-ligand in the LnCd fragment performs a chelating function on the Cd1 atom. The phenanthroline molecules coordinated by the Cd1 and Eu1 atoms are located in parallel planes, almost perpendicular to the plane of the metal atoms. They participate in an intramolecular $\pi\cdots\pi$ interaction the geometric parameters of which allow us to assume its significant strength (Table S2). The peripheral ligand in this linear compound is a chelated pfb ligand. The molecular packaging in the crystal is a zigzag chain parallel to the a axis formed by overlapping of the phenanthroline fragments of the neighboring molecules. The further development of crystal packaging is due to weaker interactions (Tables S2–S4).

Thus, our analysis of the molecular and crystal structure of compounds I–X has shown that the fragment of two lanthanide atoms and four pentafluorobenzoate fragments has the same structure regardless of its environment. Only the angle of the pentafluorobenzene rings rotation differs because of the high mobility of C–C bonds. It is also evident in the disordering of these fragments in the resulting structures, and has no effect on the geometry of the metal core. It has also been shown that the main structure-forming non-covalent interactions in the crystals studied are interactions involving the π systems of pentafluorobenzoate and phenanthroline ligands. These interactions determine both the molecular and crystal structure of the studied complexes.

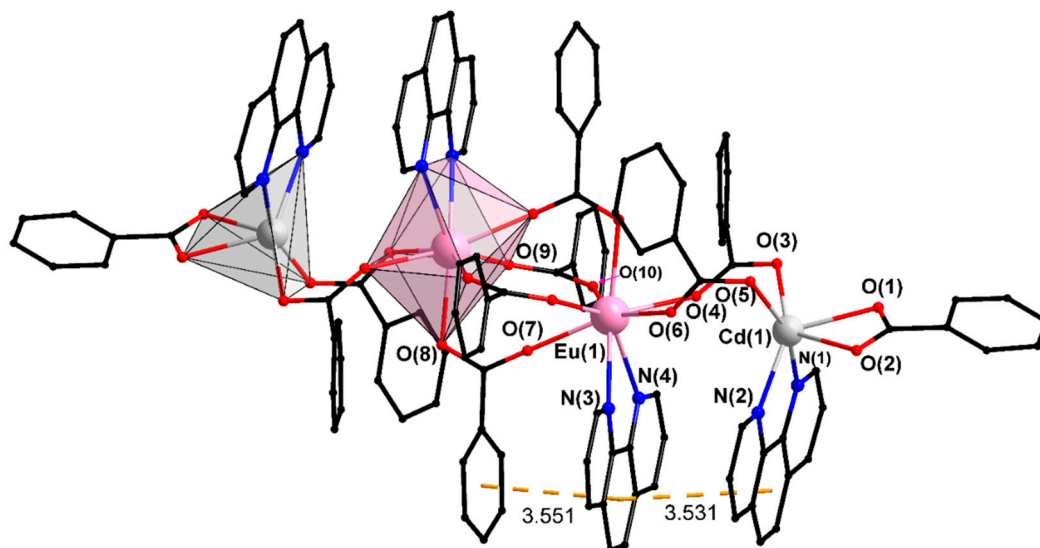


Figure 4. Structure of complex X. Hydrogen and fluorine atoms as well as solvate molecules are omitted.

2.2. Photoluminescence

The luminescence properties of the solid-state europium, terbium and gadolinium compounds I–III and V–VIII were studied in detail. The room temperature luminescence spectra of europium (Figure 5) and terbium (Figure 6) samples exhibit narrow f-f bands of the corresponding lanthanide ions as well as weak broad emission bands of *d*-block that are typical of heteronuclear lanthanide compounds (Figure 7) [37–39].

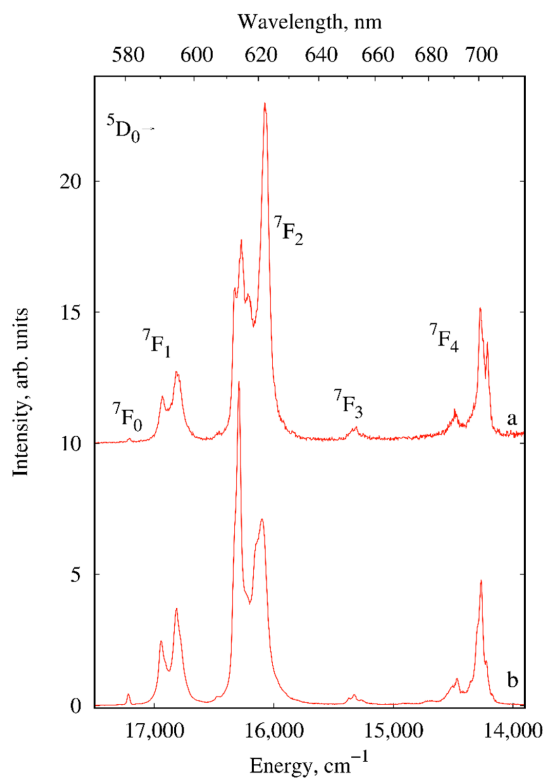


Figure 5. Luminescence spectra of I (a) and VI (b) (solid samples, $\lambda_{\text{ex}} = 280 \text{ nm}$, $T = 300 \text{ K}$).

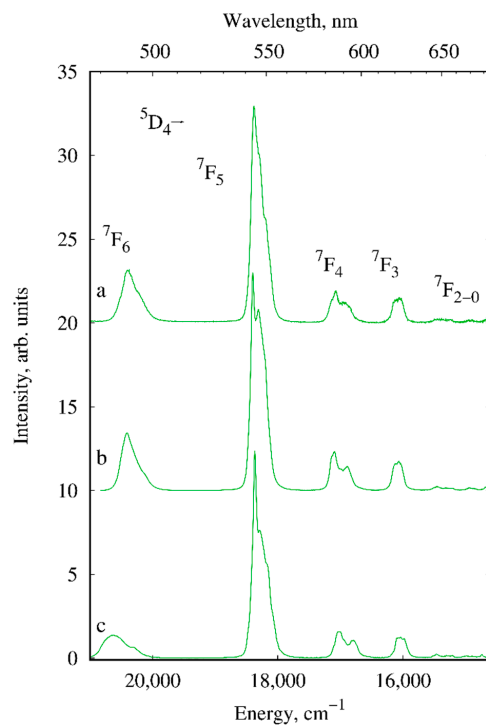


Figure 6. Luminescence spectra of III (a), V (b) and VIII (c) (solid samples, $\lambda_{\text{ex}} = 280 \text{ nm}$, $T = 300 \text{ K}$).

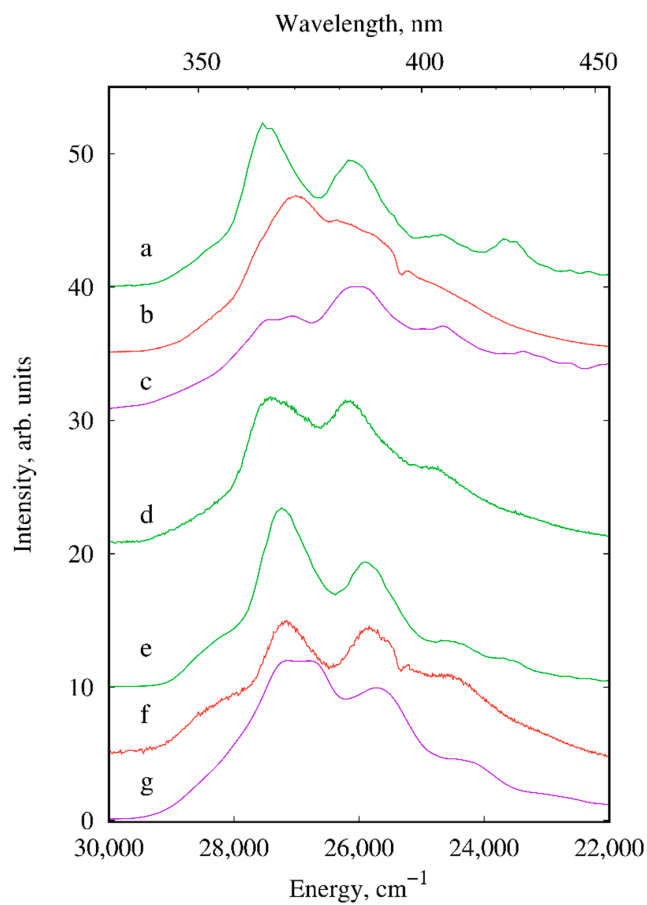


Figure 7. The d-block luminescence of III (a), I (b), II (c), V (d), VIII (e), VI (f) and VII (g) (solid samples, $\lambda_{\text{ex}} = 280 \text{ nm}$, $T = 300 \text{ K}$).

The narrow emission bands of complexes I and VI correspond to the $^5D_0 \rightarrow ^7F_J$ ($J = 0-4$) transitions of Eu^{3+} (Figure 5). The integrated intensity ratios of $^5D_0 \rightarrow ^7F_2$ hypersensitive transition to the magnetic dipole transition $^5D_0 \rightarrow ^7F_1$ of europium compounds I and VI are 4.06 and 5.97, respectively, and indicate a deviation of the Eu^{3+} site symmetry from the inversion center. The $^5D_0 \rightarrow ^7F_0$ transition displays a single symmetrical narrow component in all cases that indicates the presence of only one type of the Eu^{3+} environment. This is confirmed by the fact that all luminescence decay curves of the excited 5D_0 level of Eu^{3+} and of the excited 5D_4 level of Tb^{3+} were well fit by a monoexponential decay function (Table 3).

Table 3. Radiative (A_{rad}) and non-radiative (A_{nrad}) rate constants, luminescence lifetimes (τ), intrinsic (Q_{Ln}^{Ln}) and overall (Q_{Ln}^L) quantum yields and sensitization efficiency (η_{sens}) of I, III, IV, VI and VIII.

Compound	$A_{\text{rad}}, \text{s}^{-1}$ ^a	$A_{\text{nrad}}, \text{s}^{-1}$	τ, ms	$Q_{Ln}^{Ln}, \%$ ^a	$Q_{Ln}^L, \%$ ^b	$\eta_{\text{sens}}, \%$
I (EuCd)	325	195	1.92 ± 0.05	62	36	58
VI (Eu_2Zn_2)	425	100	1.90 ± 0.05	81	41	51
$[\text{Eu}(\text{pfb})_3(\text{H}_2\text{O})_n]$ [13]	-	-	0.65	65	15	23
III (TbCd)	-	-	2.09 ± 0.06	-	63	-
V (Tb_2Cd_2)	-	-	1.95 ± 0.06	-	33	-
VIII (Tb_2Zn_2)	-	-	1.83 ± 0.05	-	45	-
$[\text{Tb}(\text{pfb})_3(\text{H}_2\text{O})_n]$ [13]	-	-	1.36	-	38	-

^a—were measured at excitation wavelength 464 nm. ^b—were measured at excitation wavelength 280 nm.

The f-f luminescence bands of III, V and VIII are assigned to $^5D_4 \rightarrow ^7F_J$ ($J = 6-3$) transitions of Tb^{3+} (Figure 6). The emission spectra of all terbium compounds are dominated by the $^5D_4 \rightarrow ^7F_5$ transition at 545 nm responsible for the green color of luminescence. The similarity of the Stark splitting structure of the electronic transitions is indicative of the identity of the Tb^{3+} ion's nearest environment in Cd-containing compounds and insignificant differences in the Zn-containing compound.

The broad-band luminescence of *d*-block in the 340–450 nm wavelength range with a vibrational fine structure is clearly observed in emission spectra of europium, terbium, and gadolinium compounds (Figure 7). The existence of these bands in the luminescence spectra indicates an incomplete energy transfer from the *d*-block to the lanthanide ions.

The excitation spectra of I, III, V, VI and VIII recorded at room temperature are displayed in Figure 8. In addition to the S_0-S_1 transition of phen ligand with maximum at $\sim 29,000 \text{ cm}^{-1}$ and f-f transitions of the lanthanide ions the excitation spectra of molecular compounds V, VI and VIII display wide shoulders located up to $26,000 \text{ cm}^{-1}$. As the compounds characterized by the π -stacking interaction, the shoulder can be assigned to the interligand charge transfer (ILCT state) as the result of ligand charge redistribution. Moreover, the intense shoulder extended up to $24,500 \text{ cm}^{-1}$ of the europium compound VI is absent in isostructural terbium complex VIII and therefore indicates participation of low-lying ligand-to-metal charge transfer state (LMCT state) in the energy transfer processes of VI. It is noteworthy that compared with the molecular terbium compound V the energy of the first excited singlet state of the polymer III shows remarkable blue shift by about 300 cm^{-1} . The reason can also be π -stacking leading to bathochromic shift of the excitation maximum [11]. The domination of the ligand absorption bands in the excitation spectra proves effective luminescence sensitization via excitation of the ligand.

The triplet state energy of the *d*-block was determined from the 77 K phosphorescence spectra of Gd compounds II and VII (Figure S10) using the short-wavelength edge corresponding to 0–0 phonon transition. So, the triplet energy of *d*-block is $21,500 \text{ cm}^{-1}$, which correlates well with the reported value of the triplet state energy of phen ligand [11]. The energy differences between the S_1 and T_1 states is about 7500 cm^{-1} , which exceeds the preferred value (5000 cm^{-1} [40]) providing the most efficient intersystem crossing. However, the charge transfer states described above can promote an increase in sensitization efficiency by acting as intermediate states in the energy transfer process.

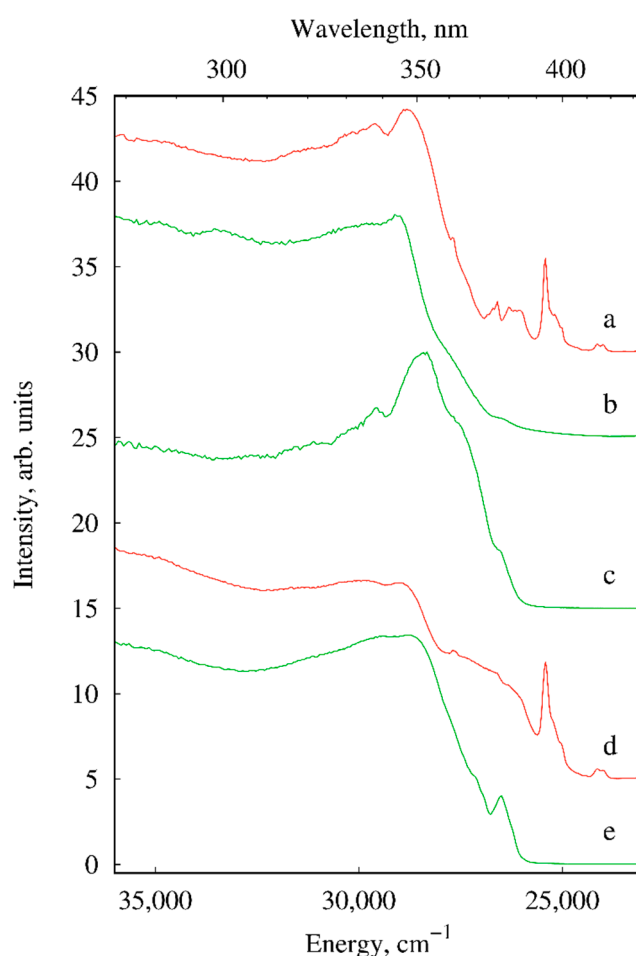


Figure 8. Excitation spectra of I (a), III (b), V (c), VI (d) and VIII (e) (solid samples, $\lambda_{em} = 615$ nm (for Eu^{3+} compounds) and 545 nm (for Tb^{3+} compounds), $T = 300$ K).

The long lifetimes (Table 3) clearly reflect a lanthanide environment devoid of water molecule. The considered quantum yields of the compounds are quite similar with the exception of terbium-containing polymer III that demonstrates a higher luminescence efficiency as well as longer lifetime of the Tb^{3+} excited state $^5\text{D}_4$. Therefore, the polymerization of III results in almost twice higher luminescence quantum yield compared to its molecular analogue V.

The long lifetimes (Table 3) clearly reflect a lanthanide environment devoid of a water molecule. The quantum yields of the compounds considered are quite similar, with the exception of terbium-containing polymer III that demonstrates a higher luminescence efficiency as well as longer lifetime of the Tb^{3+} excited state $^5\text{D}_4$. Therefore, the polymer structure of III results in an almost two times higher luminescence quantum yield compared to its molecular analogue V.

The efficiency of the energy transfer processes in the europium complexes was estimated by calculating the intrinsic quantum yields via Werts' formula [41]. The data obtained are reported in Table 3. The luminescence efficiency is essentially limited by an incomplete energy transfer from the d-block to the emission center. Nevertheless, the quantum yield of I and VI is much higher than that of homonuclear europium compounds with pfb ligands: the reported quantum yield is 15% [13]. The presence of the phen ligand result in an increase in sensitization efficiency due to more favorable energies of its excited states. Moreover, the absence of high-frequency oscillating bonds achieved by the presence of a d-block provide a significantly longer lifetime of the europium excited state regardless of the presence of phen as a ligand [5]. Since terbium luminescence is less susceptible to quenching due to a larger energy gap between the lowest excited state and the highest ground state levels, the lifetime difference between heteronuclear and homonuclear terbium compounds is less significant [42].

2.3. Magnetic Properties

The magnetic properties of complexes II–IV and VII–IX were studied in the temperature range of 2–300 K in a 5000 Oe dc-magnetic field (Figure 9; the $\chi_M T$ values for II–IV were calculated in terms of the Ln_2Cd_2 unit for clarity). The $M(H)$ and $M(H/T)$ plots for II–IV and VII–IX are shown in Figures S11–S16. The $\chi_M T(T)$ plots are similar for complexes with identical lanthanides ions. On cooling from room temperature to 2 K, the $\chi_M T$ values for II–IV, VII–IX remain nearly constant up to 9 K (II, VII) or 150 K (II, IV, VIII, IX). On further cooling, first a slow decrease and then a sharp drop in $\chi_M T$ followed by a decrease to minimum values at 2 K occurs (Figure 9). The most indicative $\chi_M T$ values are presented in Table 4, along with theoretical ones for the corresponding isolated Ln^{3+} ions. The experimental $\chi_M T$ values for complexes II–IV and VII–IX (see Table 4) are in good agreement with the theoretical ones.

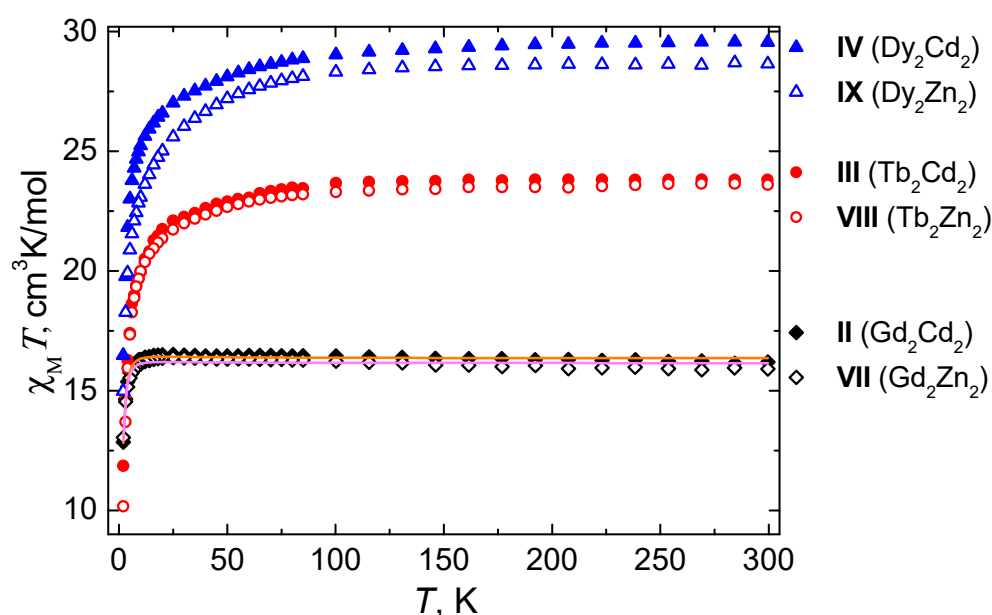


Figure 9. The $\chi_M T$ vs. T dependencies for complexes II–IV (calculated per Ln_2Cd_2 unit) and VII–IX under 5000 Oe dc-magnetic field. Solid lines are the best-fit curves obtained for complexes II and VII using PHI program [43].

Table 4. The $\chi_M T$ values of II–IV (calculated per Ln_2Cd_2 unit), VII–IX.

Complex	$\chi_M T$, $\text{cm}^3/\text{mol K}$		
	Experimental (300 K)	Theor. (2Ln) [43]	Experimental (2 K)
II	16.19	15.76	12.86
III	23.80	23.64	11.87
IV	29.55	28.34	16.47
VII	15.91	15.76	13.04
VIII	23.59	23.64	10.17
IX	28.64	28.34	14.97

With an eye to evaluate the magnitude of magnetic interactions in II and VII, the temperature dependences of $\chi_M T$ were fitted (Tables 5, S7 and S8, Figures 9, S11 and S12) using the PHI program developed by Chilton et al. [44] using $\hat{H} = J\hat{S}_1\hat{S}_2 + \mu_B g B(\hat{S}_1 + \hat{S}_2)$ Hamiltonian, where $\hat{S}_1 = \hat{S}_2 = \hat{S}_{\text{Gd}}$, J is the intramolecular magnetic exchange constant, g is the g -factor, B is the magnetic flux density, and μ_B is the Bohr magneton.

Table 5. Approximation parameters of $\chi_{MT}(T)$ dependences for complexes II and VII calculated by means of the PHI program [44].

Parameter	II	VII
	Value	
g	2.0375 ± 0.0008	2.024 ± 0.001
J, cm^{-1} (intramolecular interactions)	-0.074 ± 0.001	-0.070 ± 0.003
zJ, cm^{-1} (intermolecular interactions)	0.0204 ± 0.0006	0.020 ± 0.001
R^2	0.9968	0.9870

Intermolecular interactions (zJ) between Gd atoms were also considered using the mean-field approximation:

$$\chi_{zJ} = \frac{\chi_{calc}}{1 - \left(\frac{zJ}{N_A \mu_B^2}\right) \chi_{calc}}$$

where χ_{zJ} is the refined magnetic susceptibility based on intermolecular interaction, χ_{calc} is the magnetic susceptibility calculated on the basis of the Hamiltonian, N_A is the Avogadro number, and μ_B is the Bohr magneton. The calculation errors were estimated as

$$R = \sum_{i=1}^n (\chi_{exp} - \chi_{calc})^2$$

where n is a number of experimental points.

According to the values of intra- and intermolecular interactions presented in Table 5, one can assume that the magnetic interaction between the Gd³⁺ ions is relatively weak and cannot considerably change the magnetic behavior of complexes II and VII. The values of the exchange coupling parameters are comparable with those observed for binuclear gadolinium complexes with a similar structure [45,46].

Slow relaxation of magnetization, which has a number of promising practical applications, is often observed in lanthanide complexes, especially in Dy-containing ones. In order to study the magnetic behavior dynamics of the complexes, the magnetic susceptibility in an alternating magnetic field (ac-magnetic susceptibility) was investigated. In zero dc-magnetic field, a significant signal on the frequency plots of the imaginary component (out-of-phase signal) of ac-magnetic susceptibility $\chi''(\nu)$ was observed only for complexes containing Dy (IV and IX); however, the peak is out of the frequency range of the equipment used (10–10,000 Hz). Therefore, the evaluation of the relaxation characteristics of these complexes does not seem possible. For all the other complexes, the deviations from zero in the $\chi''(\nu)$ plots are within the measurement error of the magnetometer. Such a behavior is often associated with the dominant influence of the quantum tunneling of magnetization (QTM) relaxation process. The QTM significantly accelerates relaxation, making it unobservable. In order to suppress this relaxation process for complexes II-IV and VII-IX, the ac-magnetic susceptibility was studied in dc-magnetic fields of up to 5000 Oe at 2 K. The latter allowed us to obtain the frequency dependences of the real (χ') and imaginary (χ'') components of the ac-magnetic susceptibility (Figures S17–S22).

Relaxation deceleration of compound VIII is not observed at any dc-magnetic field applied (Figure S21). For complexes III and IV, despite a noticeable decrease in the magnetic relaxation rate, the maxima on the $\chi''(\nu)$ curves are outside the frequency range of the equipment used at any dc-magnetic fields (Figures S18 and S19), which does not allow determining the parameters of the relaxation processes of these compounds.

Varying the external dc-magnetic field strength made it possible to obtain the optimal values which correspond to the slowest relaxation for complexes II (1000 Oe), VII (2500 Oe) and IX (1500 Oe) (Figures S17, S20 and S22). By applying optimal fields, the frequency dependences of the real (χ') and imaginary (χ'') components of the ac-magnetic susceptibility (Figures 10, S23 and S24) were obtained in different temperature ranges. Based on these results, the $\chi''(\nu)$ isotherms were approximated using

the generalized Debye model and dependences of the relaxation time on the reciprocal temperature $\tau(1/T)$ for compounds II, VII, IX (Figures 11, S25 and S26) were obtained.

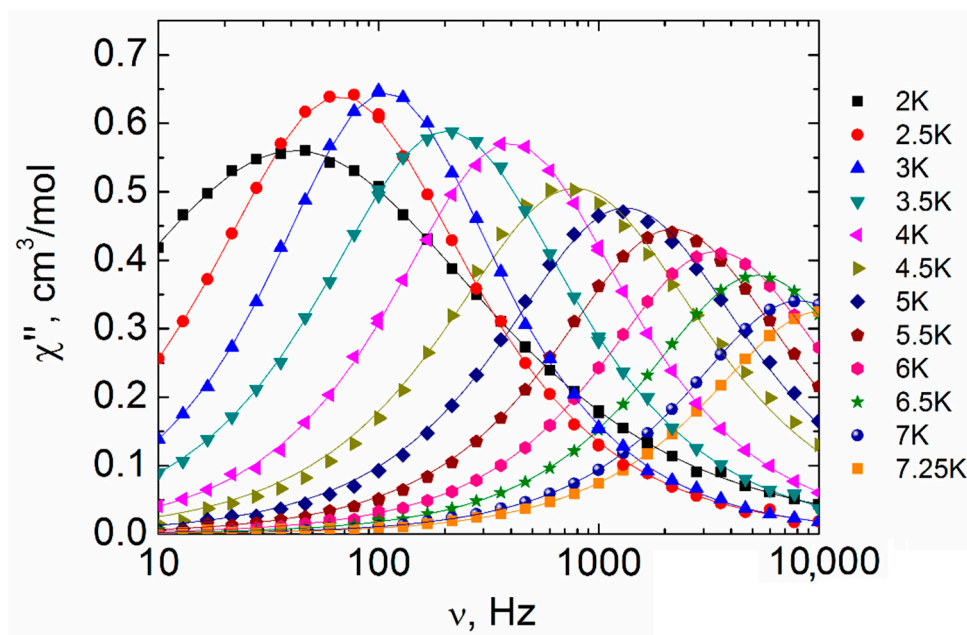


Figure 10. Frequency dependencies of the imaginary components of the ac-magnetic susceptibility for complex IX in the 2–7.25 K range taken under the optimal 1500 Oe dc-field. Solid lines represent fitting by the generalized Debye model.

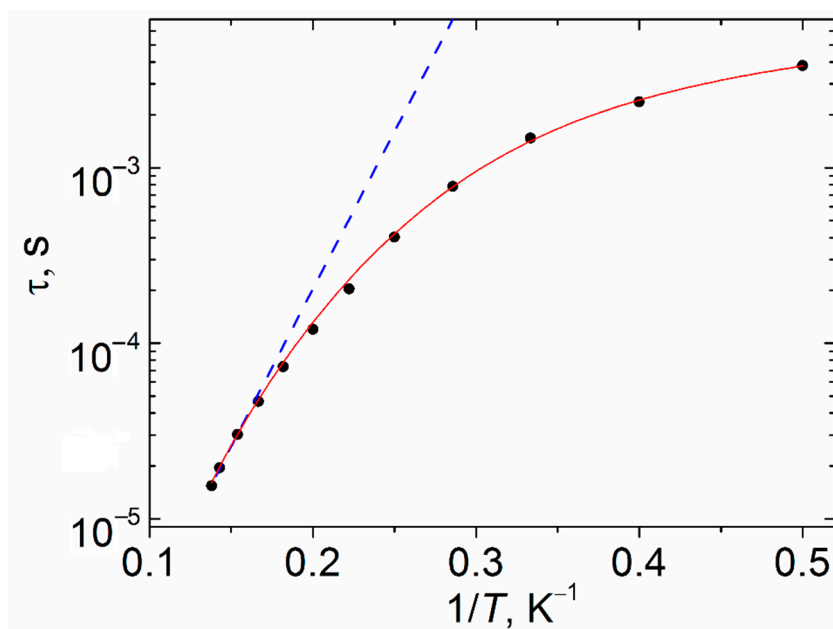


Figure 11. The τ vs. $1/T$ plot for complex IX under 1500 Oe field at $T = 2$ K. Blue dashed line represents fitting by the Orbach mechanism (Arrhenius equation). Solid red line represents fitting by the sum of direct and Raman relaxation mechanisms.

It is important to note that an increase in the intensity of $\chi''(\nu)$ signal was observed for IX with a rise in temperature from 2 K to 3 K (Figure 10). This pattern may be due to the collective behavior caused by the weak dipole-dipole or exchange interactions between the Ln^{3+} ions [3,47–52].

To determine the parameters of the relaxation processes of the compounds, the high-temperature part of the τ (1/T) dependences were approximated by the Orbach relaxation mechanism:

$$\tau_{\text{Or}}^{-1} = \tau_0^{-1} \exp(-\Delta E/k_B T) \quad (1)$$

where ΔE —effective energy barrier; k_B —Boltzmann constant, τ_0 —preexponential factor, T —temperature.

A similar estimation of the relaxation parameters of Gd-containing complexes II and VII in the temperature ranges of 5–6 K (II) and 5.5–6.5 K (VII) gives the following values: for II— $\tau_0 = 9 \times 10^{-6} (\pm 2 \times 10^{-6})$ s, $\Delta E/k_B = 4 (\pm 1)$ K; for VII— $\tau_0 = 9.8 \times 10^{-6} (\pm 5 \times 10^{-7})$ s, $\Delta E/k_B = 4.1 (\pm 0.3)$ K. For compound IX, the relaxation parameters for the temperature range 6.5–7.25 K are $\tau_0 = 5 \times 10^{-8} (\pm 1 \times 10^{-8})$ s and $\Delta E/k_B = 41 (\pm 2)$ K. The plots of $\tau(1/T)$ dependences for complexes II, VII and IX in a semilogarithmic coordinate system are nonlinear (Figures 11, S25 and S26). This indicates the presence of relaxation mechanisms that are different from the Orbach one.

It should be borne in mind that the Orbach relaxation mechanism often does not contribute to relaxation, as previously observed in a number of examples for Er and Yb complexes [52]. The latter is suggested by the τ_0 values and also by approximation of the $\tau(1/T)$ plot by the sum of the Raman and QTM relaxation mechanisms ($\tau^{-1} = C_{\text{Raman}} T^{n_{\text{Raman}}} + B$; for complexes II and VII) or Raman and direct relaxation mechanisms ($\tau^{-1} = C_{\text{Raman}} T^{n_{\text{Raman}}} + A_{\text{direct}} T^{4_{\text{direct}}}$; for complex IX) over the entire temperature range. The relaxation times characteristic of over-barrier magnetization reversal corresponding to the Orbach mechanism should be $\sim 10^{-10}$ – 10^{-12} s [53]. The τ_0 parameters of complexes II, VII, IX differ significantly from the indicated values. By using a sum of the QTM and Raman mechanisms in the approximation of the experimental data (Figures 11, S25 and S26), the following relaxation parameters were obtained: for II— $C_{\text{Raman}} = 2143 (\pm 508) \text{ K}^{-n_{\text{Raman}}} \text{ s}^{-1}$, $n_{\text{Raman}} = 1.6 (\pm 0.1)$, $B = 24,360 (\pm 1149) \text{ s}^{-1}$; for VII, $C_{\text{Raman}} = 731 (\pm 499) \text{ K}^{-n_{\text{Raman}}} \text{ s}^{-1}$, $n_{\text{Raman}} = 2.2 (\pm 0.4)$, $B = 15,938 (\pm 1973) \text{ s}^{-1}$; for complex IX, the optimal approximation was achieved using the sum of the Raman and direct relaxation mechanisms with parameters: $C_{\text{Raman}} = 0.6 (\pm 0.2) \text{ K}^{-n_{\text{Raman}}} \text{ s}^{-1}$, $n_{\text{Raman}} = 5.8 (\pm 0.2)$, $A_{\text{direct}} = 2.26 \times 10^{-11} (\pm 5 \times 10^{-13}) \text{ K}^{-1} \text{ Oe}^{-4} \text{ s}^{-1}$, $n_{\text{direct}} = 4$ (fixed for Kramers ions). The use of other sets of the mechanisms than those presented above for approximation results in over-parameterization.

3. Discussion

The fact that polymer complexes I–IV formed was found to be somewhat unexpected, since the formation of molecular structures is typical of M-Ln (where M is a transition metal) compounds with monocarboxylic acid anions and phen molecules or its substituted analogs (based on the data of CCDC (Nov. 2019 + 3 upd) [54] which describes 57 molecular compounds). Probably, the stabilization of the polymer structure is associated with non-covalent interactions in the crystal packing of the complexes, which causes the arrangement of pentafluorophenyl substituents of carboxylate anions and coordinated phen molecules to be close to parallel. Due to this mutual orientation of aromatic fragments, the carboxylate ligand coordinated by the Cd atom participates in the formation of π - π interactions with the phen molecule of the neighboring Ln_2Cd_2 fragment, while the O atom in its composition performs the μ_2 -bridging function between two cadmium atoms.

A similar bonding of mononuclear fragments accompanied by the mutual orientation of aromatic rings was previously observed for cadmium pentafluorobenzoate complexes $[\text{Cd}(\text{H}_2\text{O})(\text{bpy})(\text{pfb})_2]_n$ (where bpy–2,2'-bipyridine) [32], $[\text{Cd}(\text{phen})(\text{pfb})_2]_n$ [55], and $[\text{Eu}_2(\text{H}_2\text{O})_2\text{Cd}(\text{etpy})(\text{pfb})_8]_n$ (where etpy–3-ethynylpyridine) [28]. As we have already noted, we were unable to isolate the pure phase of molecular complex V or its analogs comprising other lanthanides. This is an interesting case for comparing the photophysical characteristics of molecular and polymeric compounds with the same composition. In addition, the availability of a sufficient amount of a pure sample of molecular complex V would make it possible to study the possibility of transition of V to III in a thermolysis process, taking DSC and XRD data into account.

Magnetic measurements showed that gadolinium (II and VII) and dysprosium (IX) complexes behave as field-induced SMM. The gadolinium(III) complexes can exhibit magnetic relaxation [56–60] either due to weak anisotropy [56] or a low rate of relaxation processes other than Orbach relaxation. The observed effect requires more thorough studies. Dysprosium-containing binuclear carboxylates were previously discussed [61] with cinnamate derivatives $[\text{Dy}_2(\text{L})_6(\text{DMSO})_2(\text{H}_2\text{O})_2]$ (where L is 3-methoxycinnamate or 2-methoxycinnamate) with coordination geometry of Dy atoms (DyO_9) described as a capped square antiprism as examples. They relax through a combination of the Raman and direct processes; the Orbach relaxation is also involved but was found to be negligible. Tuning of the coordination environment of the dysprosium atom with N-donor chelate ligands (phen or bpy) in binuclear 4-chlorobenzoates (DyO_6N_2 -square antiprism) [62] or phenoxyacetate (DyO_7N_2 -muffin) [63] led to the predominance of the Orbach relaxation process in magnetic relaxation for the former. The geometry of the DyO_9 polyhedron in the complexes described above corresponds to a muffin or a triangular dodecahedron. These results show an essential role of the coordination geometry of Dy(III) ions (preference is given to a square antiprism) in determining the type of magnetic relaxation.

4. Experimental

4.1. Materials and Methods

The new compounds were synthesized in the air using acetonitrile (MeCN, C. P.) as solvents. Following reagents were used as received in synthetic procedures: $\text{Eu}(\text{NO}_3)_3 \cdot 6\text{H}_2\text{O}$ (99.99%, «Lanhit»), $\text{Tb}(\text{NO}_3)_3 \cdot 6\text{H}_2\text{O}$ (99.99%, «Lanhit»), $\text{Gd}(\text{NO}_3)_3 \cdot 6\text{H}_2\text{O}$ (99.99%, «Lanhit»), $\text{Dy}(\text{NO}_3)_3 \cdot 5\text{H}_2\text{O}$ (99.99%, «Lanhit»), $\text{H}(\text{pfb})$ (99%, «P&M Invest»), $\text{phen} \cdot \text{H}_2\text{O}$ (99%, «Alfa Aesar»). $[\{\text{Cd}(\text{H}_2\text{O})_4(\text{pfb})\}^+_n \cdot n(\text{pfb})^-]$ [28] and $[\text{Ln}_2(\text{pfb})_6(\text{H}_2\text{O})_8] \cdot 2\text{H}_2\text{O}$ [13,36] were synthesized according to the previously reported procedures. $\text{Zn}(\text{OH})_2$ was synthesized by the reaction of stoichiometric amounts of KOH and $\text{Zn}(\text{NO}_3)_2 \cdot 6\text{H}_2\text{O}$ in water.

IR spectra of the complexes were recorded using a Perkin Elmer Spectrometer 65 (PerkinElmer, Waltham, MA, USA) equipped with a Quest ATR Accessory (Specac) by means of attenuated total reflectance (ATR) in the range of $4000\text{--}400\text{ cm}^{-1}$. C, H, N, S-analysis of the presented complexes was performed on a EuroEA 3000 device (Eurovector, Via Fratelli Cuzio, Italy).

The excitation and emission spectra were measured with a Fluorolog FL3-22 (Horiba-Jobin-Yvon) spectrofluorimeter (Horiba Scientific, Kyoto, Japan) equipped with a xenon lamp (450 W) and a R-928 photomultiplier (Hamamatsu Photonics, Hamamatsu, Japan). The spectra were corrected for instrumental responses. Lifetimes were measured with the same instrument using a xenon flash lamp. The overall quantum yields (QY) were determined by absolute method using a Spectralone-covered G8 integration sphere (GMP SA, Renens, Switzerland) coupled to the spectrofluorimeter.

Magnetic susceptibility measurements were carried out using a Quantum Design PPMS-9 susceptometer (Quantum Design, San Diego, CA, USA). The static magnetic susceptibility was measured at a magnetic field strength of 5000 Oe in the temperature range of 2–300 K. Alternating field measurements were performed at 1, 3 and 5 Oe in a frequency range of 10–10,000 Hz. All polycrystalline samples for the magnetic measurements were placed in polyethylene packs and mixed with an inert mineral oil to preclude the orientation of the crystals in magnetic field. In magnetic susceptibility calculations, the paramagnetic components of χ were determined with respect to the sample holder and mineral oil contributions and the diamagnetic contribution of the sample estimated from Pascal's constants.

Single crystal X-Ray diffraction experiments with I-X were done on a Bruker Apex II diffractometer (Bruker, Billerica, MA, USA) with a CCD camera and a graphite monochromated $\text{MoK}\alpha$ radiation source ($\lambda = 0.71073\text{ \AA}$) [64]. Semiempirical absorption corrections were used in all the experiments [65]. Direct methods and Fourier techniques were used in structure solving. The refinement was done by the full-matrix least squares technique against F^2 with anisotropic thermal parameters for all non-hydrogen atoms. The H atoms of the hydroxy groups were calculated by difference Fourier

synthesis and geometrically in the other cases. The H atoms in the structures were refined in the riding model. Using Olex2, [66] the structure was solved by direct methods in the ShelXS program package. The structures were refined by ShelXL [67]. The SHAPE 2.1 software [68] was used to determine the metals polyhedrons. The most important experimental crystallographic data and refinement statistics are reported in Tables S5 and S6. Supplementary crystallographic data for the compounds synthesized are given in CCDC numbers 2035046 (for I), 2035047 (for II), 2035048 (for III), 2035049 (for IV), 2035050 (for V), 2035051 (for VI), 2035052 (for VII), 2035053 (for VIII), 2035055 (for IX), 2036917 (for X). These data can be obtained free of charge from The Cambridge Crystallographic Data Centre via www.ccdc.cam.ac.uk/data_request/cif.

The PXRD data in the form of powder patterns were collected on a Bruker D8 Advance diffractometer (Bruker, Billerica, MA, USA) with a LynxEye detector in Bragg-Brentano geometry, with the sample thinly dispersed on a zero-background Si sample holder, $\lambda(\text{CuK}\alpha) = 1.54060 \text{ \AA}$, θ/θ scan with variable slits (irradiated length 20 mm), 2θ from 5° to 41° , step size 0.02° .

4.2. Synthesis

$[\text{LnCd}(\text{pfb})_5(\text{phen})]_n \cdot 1.5n\text{MeCN}$ (*Eu(I)*, *Gd(II)*, *Tb(III)*, *Dy(IV)*).

Compound $[\text{Ln}_2(\text{pfb})_6(\text{H}_2\text{O})_8] \cdot 2\text{H}_2\text{O}$ (0.083 mmol, Ln = Eu(I), Gd(II), Tb(III), Dy(IV)) was added to a solution of $[\{\text{Cd}(\text{H}_2\text{O})_4(\text{pfb})\}^+_{n \cdot n}(\text{pfb})^-]$ (0.100 g, 0.166 mmol) in 5 mL MeCN. The reaction mixture was stirred at 75°C for 20 min, then 0.029 g of phen (0.166 mmol) was added. The solution was kept in a sealed vial at room temperature. Colorless crystals suitable for X-ray diffraction studies that precipitated after 7 days were filtered off, washed with cold MeCN ($T = 5^\circ\text{C}$), and dried in air at 20°C .

The yield of I was 0.177 g (68.9%) based on $[\{\text{Cd}(\text{H}_2\text{O})_4(\text{pfb})\}^+_{n \cdot n}(\text{pfb})^-]$. Anal. Calc. for $\text{C}_{50}\text{H}_{12.5}\text{O}_{10}\text{N}_{3.5}\text{F}_{25}\text{EuCd}$ (%): C 38.5; H 0.8; N 3.1. Found(%): C 38.3; H 0.5; N 2.9. IR (ATR), ν/cm^{-1} : 1649 m, 1627 m, 1589 s, 1574 m, 1518 m, 1488 s, 1449 m, 1433 m, 1384 s, 1348 m, 1283 m, 1222 w, 1136 m, 1103 s, 990 s, 930 m, 864 m, 846 m, 826 m, 759 s, 725 s, 696 s, 650 m, 639 m, 619 w, 556 w, 545 w, 504 m.

The yield of II was 0.209 g (81.4%) based on $[\{\text{Cd}(\text{H}_2\text{O})_4(\text{pfb})\}^+_{n \cdot n}(\text{pfb})^-]$. Anal. Calc. for $\text{C}_{50}\text{H}_{12.5}\text{O}_{10}\text{N}_{3.5}\text{F}_{25}\text{GdCd}$ (%): C 38.3; H 0.8; N 3.1. Found(%): C 38.3; H 0.6; N 3.0. IR (ATR), ν/cm^{-1} : 1649 m, 1627 m, 1589 s, 1574 m, 1518 m, 1488 s, 1449 m, 1433 m, 1384 s, 1345 m, 1284 m, 1283 w, 1221 w, 1136 m, 1103 s, 989 s, 930 m, 864 m, 846 m, 823 m, 759 s, 725 s, 697 s, 650 m, 640 m, 619 w, 556 w, 546 w, 505 m.

The yield of III was 0.200 g (78.1%) based on $[\{\text{Cd}(\text{H}_2\text{O})_4(\text{pfb})\}^+_{n \cdot n}(\text{pfb})^-]$. Anal. Calc. for $\text{C}_{50}\text{H}_{12.5}\text{O}_{10}\text{N}_{3.5}\text{F}_{25}\text{TbCd}$ (%): C 38.3; H 0.8; N 3.1. Found(%): C 38.4; H 0.7; N 3.3. IR (ATR), ν/cm^{-1} : 1649 m, 1627 m, 1589 s, 1574 m, 1518 m, 1488 s, 1449 m, 1433 m, 1384 s, 1348 m, 1284 m, 1283 w, 1222 w, 1136 m, 1103 s, 990 s, 930 m, 864 m, 846 m, 826 m, 759 s, 725 s, 696 s, 650 m, 640 m, 619 w, 556 w, 546 w, 505 m.

The yield of IV was 0.170 g (67.5%) based on $[\{\text{Cd}(\text{H}_2\text{O})_4(\text{pfb})\}^+_{n \cdot n}(\text{pfb})^-]$. Anal. Calc. for $\text{C}_{50}\text{H}_{12.5}\text{O}_{10}\text{N}_{3.5}\text{F}_{25}\text{DyCd}$ (%): C 38.2; H 0.8; N 3.1. Found: C 38.3; H 0.9; N 3.0. IR (ATR), ν/cm^{-1} : 1651 m, 1627 w, 1589 s, 1569 m, 1519 w, 1488 m, 1450 m, 1433 m, 1384 s, 1348 m, 1285 m, 1288 m, 1222 w, 1139 w, 1099 w, 991 s, 925 w, 864 m, 845 m, 826 m, 755 s, 725 s, 701 m, 650 m, 638 m, 619 w, 553 w, 547 w, 505 m.

$[\text{Tb}_2\text{Cd}_2(\text{phen})_2(\text{pfb})_{10}](\text{V})$.

Complex V was synthesized as described above for compound III. The resulting reaction mixture was kept in a sealed vial at 75°C . Colorless crystals suitable for X-ray diffraction studies that precipitated after 2 days were filtered off, washed with cold MeCN ($T = 5^\circ\text{C}$), and dried in air at 20°C . The yield of V was 0.109 g (42.5%) based on $[\{\text{Cd}(\text{H}_2\text{O})_4(\text{pfb})\}^+_{n \cdot n}(\text{pfb})^-]$. Anal. Calc. for $\text{C}_{94}\text{H}_{16}\text{O}_{20}\text{N}_4\text{F}_{50}\text{Tb}_2\text{Cd}_2$ (%): C 37.6; H 0.5; N 1.9. Found: C 37.3; H 0.4; N 1.7. IR-spectra (ATR), ν/cm^{-1} : 1723 m, 1698 m, 1651 m, 1613 s, 1520 s, 1490 s, 1430 m, 1390 s, 1316 m, 1227 m, 1140 w, 1103 s, 989 s, 929 m, 855 w, 844 s, 831 m, 761 m, 741 s, 725 s, 707 s, 642 m, 584 w, 504 w.

$[\text{Ln}_2\text{Zn}_2(\text{phen})_2(\text{pfb})_{10}] \cdot 4\text{MeCN}$ (*Ln = Eu(VI)*, *Gd(VII)*, *Tb(VIII)*, *Dy(IX)*).

0.314 g of H(pfb) (1.485 mmol) was added to as-precipitated Zn(OH)₂ (0.075 g, 0.742 mmol) in 20 mL H₂O. The reaction mixture was stirred at 75 °C for 2 h until complete dissolution of Zn(OH)₂ and evaporated to dryness. The precipitate that formed was dissolved in 15 mL of MeCN, then [Ln₂(pfb)₆(H₂O)₈]·2H₂O (0.371 mmol, Ln = Eu(VI), Gd(VII), Tb(VIII), Dy(IX)) was added to the resulting solution. The reaction mixture was kept in a sealed vial at room temperature. Colorless crystals suitable for X-ray diffraction studies that precipitated after 3 days were filtered off, washed with cold MeCN (T = 5 °C), and dried in air at 20 °C.

The yield of VI was 0.948 g (83.3%) based on Zn(OH)₂. Anal. Calc. for C₁₀₂H₂₈O₂₀N₈F₅₀Eu₂Zn₂ (%): C 39.9; H 0.9; N 3.7. Found: C 40.1; H 1.0; N 3.9. IR (ATR), ν/cm^{-1} : 1723 m, 1698 m, 1651 m, 1613 s, 1521 s, 1490 s, 1427 m, 1396 s, 1316 m, 1225 m, 1147 w, 1103 s, 988 s, 932 m, 855 w, 844 s, 831 m, 761 m, 741 s, 725 s, 707 s, 640 m, 583 w, 507 w.

The yield of VII was 0.895 g (78.6%) based on Zn(OH)₂. Anal. Calc. for C₁₀₃H₃₂O₂₂N₈F₅₀Gd₂Zn₂ (%): C 39.3; H 1.0; N 3.6. Found: C 39.2; H 1.3; N 3.8. IR (ATR), ν/cm^{-1} : 1721 m, 1651 m, 1613 s, 1521 s, 1489 s, 1427 m, 1390 s, 1293 m, 1225 m, 1144 w, 1107 s, 1049 w, 990 s, 932 m, 854 w, 848 s, 827 m, 769 m, 755 m, 741 s, 725 s, 698 s, 635 m, 583 w, 507 w.

The yield of VIII was 0.651 g (58.5%) based on Zn(OH)₂. Anal. Calc. for C₁₀₂H₂₈O₂₀N₈F₅₀Tb₂Zn₂ (%): C 39.7; H 0.9; N 3.6. Found: C 39.5; H 0.8; N 3.7. IR (ATR), ν/cm^{-1} : 1721 m, 1651 m, 1613 s, 1521 s, 1489 s, 1427 m, 1392 s, 1293 m, 1225 m, 1147 w, 1107 s, 1047 w, 990 s, 932 m, 855 w, 848 s, 827 m, 769 m, 755 m, 741 s, 725 s, 697 s, 635 m, 583 w, 506 w.

The yield of IX was 0.700 g (61.1%) based on Zn(OH)₂. Anal. Calc. for C₁₀₂H₂₈O₂₀N₈F₅₀Dy₂Zn₂ (%): C 39.6; H 0.9; N 3.6. Found: C 39.8; H 0.8; N 3.5. IR (ATR), ν/cm^{-1} : 1720 w, 1652 m, 1613 s, 1521 s, 1490 s, 1427 m, 1392 s, 1296 m, 1225 w, 1149 w, 1106 s, 1047 m, 990 s, 930 w, 855 w, 848 m, 827 m, 769 m, 750 m, 738 m, 725 s, 699 s, 635 m, 583 w, 500 w.

[Eu₂Cd₂(phen)₄(pfb)₁₀]·4MeCN (X).

0.157 g of H(pfb) (0.742 mmol) was added to as-precipitated Zn(OH)₂ (0.038 g, 0.371 mmol) in 20 mL H₂O. The reaction mixture was stirred at 75 °C for 2 h until complete dissolution of Zn(OH)₂ and evaporated to dryness. The precipitate that formed was dissolved in 40 mL of MeCN, then [(Cd(H₂O)₄(pfb))_n⁺·n(pfb)⁻] (0.224 g, 0.371 mmol), [Eu₂(pfb)₆(H₂O)₈]·2H₂O (0.650 g, 0.742 mmol) and phen (0.267 g, 1.484 mmol) were added to the resulting solution. The reaction mixture was stirred for 5 min and left to evaporate slowly at 75 °C. Colorless crystals suitable for X-ray diffraction studies that precipitated after 5 days were filtered off, washed with cold MeCN (T = 5 °C), and dried in air at 20 °C. The yield of X was 0.150 g (22.3%) based on [(Cd(H₂O)₄(pfb))_n⁺·n(pfb)⁻]. Anal. Calc. for C₁₂₆H₄₄O₂₀N₁₂F₅₀Eu₂Cd₂ (%): C 42.9; H 1.3; N 4.8. Found: C 43.3; H 1.6; N 4.7. IR (ATR), ν/cm^{-1} : 3659 w, 2988 w, 2901 w, 1647 m, 1591 m, 1518 m, 1486 s, 1427 s, 1383 s, 1294 w, 1224 w, 1137 w, 1105 m, 989 s, 930 m, 865 w, 846 m, 826 m, 747 s, 725 s, 696 m, 640 m, 582 m, 506 m, 484 w, 462 w.

5. Conclusions

A series of new M-Ln (M = Zn, Cd, Ln = Eu, Gd, Tb, Dy) heterometallic complexes with pentafluorobenzoic acid anions and 1,10-phenanthroline were synthesized. For the Cd-Ln complexes, the possibility of obtaining 1D polymers at RT and molecular complexes at 75 °C (for complex V as an example) was revealed, the composition of which differs only in the presence of acetonitrile solvate molecules for I–IV. At the same time, LnZn complexes form molecular compounds under similar conditions. The peculiarity of the formation of the polymeric LnCd structure is due to the lability of the carboxylate group, the functionality of which changes from μ_2, η_2 to μ_3, η_2 on passage from the molecular to polymeric form of the complex, and the accompanying enhancement of intramolecular π - π interactions between aromatic fragments (pfb anion and 1,10-phenanthroline) of neighboring tetranuclear fragments. Europium and terbium containing complexes exhibit bright metal-centered emission in the red and green regions, respectively. The luminescence efficiency is essentially limited by incomplete energy transfer from *d*-block to the emission center, but the presence of the phen ligand, the absence of H₂O molecules (that are usually present in the composition of the lanthanide

carboxylates) as well as high-frequency oscillating bonds achieved by the presence of *d*-block provide longer lifetimes of europium and terbium excited states and higher quantum yields (for the EuM complexes) than those of homonuclear europium and terbium perfluorobenzoates. The Gd(III) ions bound by carboxylate ligands in complexes II and VII cause very weak antiferromagnetic coupling between them. Complexes II-IV, VII and IX exhibit magnetic relaxation at helium temperatures in nonzero magnetic fields, but only for II, VII and IX the maxima on the curves $\chi''(\nu)$ are in the frequency range of the equipment used. The magnetic relaxation of gadolinium compounds II and VII is associated with the QTM and Raman mechanisms. For dysprosium complex IX, magnetic relaxation is approximated by a sum of the Raman and direct relaxation mechanisms.

Supplementary Materials: The following are available online at <http://www.mdpi.com/1996-1944/13/24/5689/s1>, Tables S1–S6 (structural data), Figures S1–S9 (PXRD data), Figure S10 (Photoluminescence data), Figures S10–S26, Tables S7–S8 magnetic data.

Author Contributions: Conceptualization, validation, M.A.K., A.A.S. and N.V.G.; methodology, M.A.S., N.V.G. and A.A.S.; formal analysis, M.A.S., J.K.V., I.V.T. and N.N.E.; investigation, M.A.S., K.A.B., E.A.V. and V.M.K.; writing—original draft preparation, M.A.S., A.A.S. and I.L.E.; writing—review and editing, M.A.K.; supervision, I.L.E. All authors have read and agreed to the published version of the manuscript.

Funding: This research was funded by Russian science foundation, grant number 16-13-10537.

Acknowledgments: X-ray diffraction analysis, CHN and IR-spectral analyzes, as well as magnetochemical studies were performed using the equipment at the Center for Collective Use of the Kurnakov Institute RAS, which operates with the support of the state assignment of the IGIC RAS in the field of fundamental scientific research. We are grateful to Bolotko A.E. for help in the synthesis.

Conflicts of Interest: The authors declare no conflict of interest.

References

1. Tang, J.; Wang, L.; Mao, D.; Wang, W.; Zhang, L.; Wu, S.; Xie, Y. Ytterbium pentafluorobenzoate as a novel fluororous Lewis acid catalyst in the synthesis of 2,4-disubstituted quinolines. *Tetrahedron* **2011**, *67*, 8465–8469. [[CrossRef](#)]
2. Baldoví, J.J.; Kondinski, A. Exploring High-Symmetry Lanthanide-Functionalized Polyoxopalladates as Building Blocks for Quantum Computing. *Inorganics* **2018**, *6*, 101. [[CrossRef](#)]
3. Efimov, N.N.; Koroteev, P.S.; Gavrikov, A.; Ilyukhin, A.B.; Dobrokhotova, Z.V.; Novotortsev, V.M. Magnetic Behavior of Carboxylate and β -Diketonate Lanthanide Complexes Containing Stable Organometallic Moieties in the Core-Forming Ligand. *Magnetochemistry* **2016**, *2*, 38. [[CrossRef](#)]
4. Sapijanik, A.A.; Fedin, V.P. Main Approaches to the Synthesis of Heterometallic Metal-Organic Frameworks. *Russ. J. Coord. Chem.* **2020**, *46*, 443–457. [[CrossRef](#)]
5. Han, L.-J.; Kong, Y.-J.; Sheng, N.; Jiang, X.-L. A new europium fluororous metal–organic framework with pentafluorobenzoate and 1,10-phenanthroline ligands: Synthesis, structure and luminescent properties. *J. Fluor. Chem.* **2014**, *166*, 122–126. [[CrossRef](#)]
6. Utochnikova, V.; Kuzmina, N.P. Photoluminescence of lanthanide aromatic carboxylates. *Russ. J. Coord. Chem.* **2016**, *42*, 679–694. [[CrossRef](#)]
7. Feng, X.; Guo, N.; Li, R.; Chen, H.; Ma, L.; Li, Z.; Wang, L. A facile route for tuning emission and magnetic properties by controlling lanthanide ions in coordination polymers incorporating mixed aromatic carboxylate ligands. *J. Solid State Chem.* **2018**, *268*, 22–29. [[CrossRef](#)]
8. Raj, D.B.A.; Biju, S.; Reddy, M.L.P. One-, Two-, and Three-Dimensional Arrays of Eu³⁺-4,4,5,5-pentafluoro-1-(naphthalen-2-yl)pentane-1,3-dione complexes: Synthesis, Crystal Structure and Photophysical Properties. *Inorg. Chem.* **2008**, *47*, 8091–8100. [[CrossRef](#)]
9. Eliseeva, S.V.; Bünzli, J.-C.G. Lanthanide luminescence for functional materials and bio-sciences. *Chem. Soc. Rev.* **2010**, *39*, 189–227. [[CrossRef](#)]
10. Binzli, J.C.G.; Piguet, C. Taking advantage of luminescent lanthanide ions. *Chem. Soc. Rev.* **2005**, *34*, 1048–1077. [[CrossRef](#)]
11. Puntus, L.N.; Lyssenko, K.A.; Antipin, M.Y.; Bünzli, J.C.G. Role of Inner- and Outer-Sphere Bonding in the Sensitization of Eu(III)-Luminescence Deciphered by Combined Analysis of Experimental Electron Density Distribution Function and Photophysical Data. *Inorg. Chem.* **2008**, *47*, 11095–11107. [[CrossRef](#)] [[PubMed](#)]

12. Han, Y.; Yan, P.; Sun, J.; An, G.; Yao, X.; Li, Y.-X.; Li, G. Luminescence and white-light emitting luminescent sensor of tetrafluoroterephthalate-lanthanide metal-organic frameworks. *Dalton Trans.* **2017**, *46*, 4642–4653. [[CrossRef](#)] [[PubMed](#)]
13. Kalyakina, A.S.; Utochnikova, V.; Bushmarinov, I.S.; Ananyev, I.V.; Eremenko, I.L.; Volz, D.; Röncke, F.; Schepers, U.; Van Deun, R.; Trigub, A.L.; et al. Highly Luminescent, Water-Soluble Lanthanide Fluorobenzoates: Syntheses, Structures and Photophysics, Part I: Lanthanide Pentafluorobenzoates. *Chem. Eur. J.* **2015**, *21*, 17921–17932. [[CrossRef](#)] [[PubMed](#)]
14. Kalyakina, A.S.; Utochnikova, V.; Bushmarinov, I.S.; Le-Deygen, I.M.; Volz, D.; Weis, P.; Schepers, U.; Kuzmina, N.P.; Bräse, S. Lanthanide Fluorobenzoates as Bio-Probes: A Quest for the Optimal Ligand Fluorination Degree. *Chem. Eur. J.* **2017**, *23*, 14944–14953. [[CrossRef](#)]
15. Utochnikova, V.; Solodukhin, N.N.; Aslandukov, A.N.; Marciniak, L.; Bushmarinov, I.S.; Vashchenko, A.A.; Kuzmina, N.P. Lanthanide tetrafluorobenzoates as emitters for OLEDs: New approach for host selection. *Org. Electron.* **2017**, *44*, 85–93. [[CrossRef](#)]
16. Kalyakina, A.S.; Utochnikova, V.; Zimmer, M.; Dietrich, F.; Van Deun, R.; Nieger, M.; Gerhards, M.; Schepers, U.; Bräse, S.; Kaczmarek, A.M.; et al. Remarkable high efficiency of red emitters using Eu(III) ternary complexes. *Chem. Commun.* **2018**, *54*, 5221–5224. [[CrossRef](#)]
17. Feng, X.; Shang, Y.; Zhang, H.; Li, R.; Wang, W.; Zhang, D.; Wang, L.; Li, Z. Enhanced luminescence and tunable magnetic properties of lanthanide coordination polymers based on fluorine substitution and phenanthroline ligand. *RSC Adv.* **2018**, *9*, 16328–16338. [[CrossRef](#)]
18. Yao, X.; Wang, X.; Han, Y.; Yan, P.; Li, Y.-X.; Li, G. Structure, color-tunable luminescence, and UV-vis/NIR benzaldehyde detection of lanthanide coordination polymers based on two fluorinated ligands. *CrystEngComm* **2018**, *20*, 3335–3343. [[CrossRef](#)]
19. Casanovas, B.; Font-Bardía, M.; Speed, S.; El Fallah, M.S.; Vicente, R. Field-Induced SMM and Visible/NIR-Luminescence Behaviour of Dinuclear Ln(III) Complexes with 2-Fluorobenzoate. *Eur. J. Inorg. Chem.* **2018**, *2018*, 1928–1937. [[CrossRef](#)]
20. Casanovas, B.; Speed, S.; Vicente, R.; Font-Bardía, M. Sensitization of visible and NIR emitting lanthanide(III) ions in a series of dinuclear complexes of formula $[Ln_2(\mu\text{-}2\text{-FBz})_2(2\text{-FBz})_4(\text{terpy})_2]\cdot 2(2\text{-HFBz})\cdot 2(\text{H}_2\text{O})$. *Polyhedron* **2019**, *173*, 114113. [[CrossRef](#)]
21. Shmelev, M.A.; Gogoleva, N.V.; Dolgushin, F.M.; Lyssenko, K.A.; Kiskin, M.A.; Varaksina, E.A.; Taidakov, I.V.; Sidorov, A.A.; Eremenko, I.L. Influence of Substituents in the Aromatic Fragment of the Benzoate Anion on the Structures and Compositions of the Formed $[Cd\text{-}Ln]$ Complexes. *Russ. J. Coord. Chem.* **2020**, *46*, 493–504. [[CrossRef](#)]
22. Shmelev, M.A.; Gogoleva, N.; Sidorov, A.A.; Kiskin, M.A.; Voronina, J.K.; Nelyubina, Y.V.; Varaksina, E.A.; Korshunov, V.M.; Taydakov, I.V.; Eremenko, I.L. Coordination polymers based on 3,5-di-tert-butylbenzoate $\{Cd_2Eu\}$ moieties. *Inorg. Chim. Acta* **2020**, *515*, 120050. [[CrossRef](#)]
23. Li, S.-S.; Ye, Z.-N.; Xu, S.-S.; Zhang, Y.-J.; Tao, A.-R.; Liu, M.; Zeng, C.-H.; Zhong, S. Highly luminescent lanthanide CPs based on dinuclear cluster: Crystal structure and sensitive Trp sensor. *RSC Adv.* **2015**, *5*, 71961–71967. [[CrossRef](#)]
24. Yu, H.-H.; Chi, J.-Q.; Su, Z.-M.; Li, X.; Sun, J.; Zhou, C.; Hu, X.-L.; Liu, Q. A water-stable terbium metal-organic framework with functionalized ligands for the detection of Fe^{3+} and $Cr_2O_7^{2-}$ ions in water and picric acid in seawater. *CrystEngComm* **2020**, *22*, 3638–3643. [[CrossRef](#)]
25. Sobieray, M.; Gode, J.; Seidel, C.; Poß, M.; Feldmann, C.; Ruschewitz, U. Bright luminescence in lanthanide coordination polymers with tetrafluoroterephthalate as a bridging ligand. *Dalton Trans.* **2015**, *44*, 6249–6259. [[CrossRef](#)]
26. Feng, X.; Sun, Y.-L.; Li, R.-F.; Zhang, T.; Guo, N.; Wang, L.-Y. Two novel europium coordination polymers based on fluorine substituted and similar carboxylate ligands: Syntheses, structures and luminescence. *Inorg. Chem. Commun.* **2016**, *73*, 190–195. [[CrossRef](#)]
27. Li, J.-J.; Fan, T.-T.; Qu, X.-L.; Han, H.-L.; Li, X. Temperature-induced 1D lanthanide polymeric frameworks based on L_n ($n = 2, 2, 4, 6$) cores: Synthesis, crystal structures and luminescence properties. *Dalton Trans.* **2016**, *45*, 2924–2935. [[CrossRef](#)]

28. Shmelev, M.A.; Gogoleva, N.V.; Kuznetsova, G.N.; Kiskin, M.A.; Voronina, Y.K.; Yakushev, I.A.; Ivanova, T.M.; Nelyubina, Y.V.; Sidorov, A.A.; Eremenko, I.L. Cd(II) and Cd(II)–Eu(III) Complexes with Pentafluorobenzoic Acid Anions and N-Donor Ligands: Synthesis and Structures. *Russ. J. Coord. Chem.* **2020**, *46*, 557–572. [[CrossRef](#)]
29. Shmelev, M.A.; Gogoleva, N.V.; Makarov, D.A.; Kiskin, M.A.; Yakushev, I.A.; Dolgushin, F.M.; Aleksandrov, G.G.; Varaksina, E.A.; Taidakov, I.V.; Aleksandrov, E.V.; et al. Synthesis of Coordination Polymers from the Heterometallic Carboxylate Complexes with Chelating N-Donor Ligands. *Russ. J. Coord. Chem.* **2020**, *46*, 1–14. [[CrossRef](#)]
30. Sidhu, J.S.; Sharma, R.P.; Aree, T.; Venugopalan, P. Second sphere coordination in fluoroanion binding: Synthesis, spectroscopic and X-ray structural study of [Co(phen)2CO3](Pfbz)·6H2O. *J. Fluor. Chem.* **2009**, *130*, 650–655. [[CrossRef](#)]
31. Sharma, R.P.; Saini, A.; Singh, S.; Venugopalan, P.; Harrison, W.T.A. Segregated aromatic π – π stacking interactions involving fluorinated and non-fluorinated benzene rings: Cu(py)2(pfb)2 and Cu(py)2(pfb)2(H2O) (py=pyridine and pfb=pentafluorobenzoate). *J. Fluor. Chem.* **2010**, *131*, 456–460. [[CrossRef](#)]
32. Kong, Y.-J.; Li, P.; Han, L.-J.; Fan, L.-T.; Yin, S. Two cadmium(II) fluorine coordination compounds tuned by different bipyridines. *Acta Crystallogr. Sect. C* **2017**, *73*, 424–429. [[CrossRef](#)] [[PubMed](#)]
33. Sivchik, V.V.; Solomatina, A.I.; Chen, Y.-T.; Karttunen, A.J.; Tunik, S.P.; Chou, P.-T.; Koshevoy, I.O. Halogen Bonding to Amplify Luminescence: A Case Study Using a Platinum Cyclometalated Complex. *Angew. Chem. Int. Ed.* **2015**, *54*, 14057–14060. [[CrossRef](#)] [[PubMed](#)]
34. Li, L.; Wang, H.; Wang, W.; Jin, W.J. Interactions between haloperfluorobenzenes and fluoranthene in luminescent cocrystals from π -hole $\cdots \pi$ to σ -hole $\cdots \pi$ bonds. *CrystEngComm* **2017**, *19*, 5058–5067. [[CrossRef](#)]
35. Mikhalyova, E.A.; Yakovenko, A.V.; Zeller, M.; Kiskin, M.A.; Kolomzarov, Y.V.; Eremenko, I.L.; Addison, A.W.; Pavlishchuk, V.V. Manifestation of π – π Stacking Interactions in Luminescence Properties and Energy Transfer in Aromatically-Derived Tb, Eu and Gd Tris(pyrazolyl)borate Complexes. *Inorg. Chem.* **2015**, *54*, 3125–3133. [[CrossRef](#)] [[PubMed](#)]
36. Larionov, S.V.; Glinskaya, L.A.; Leonova, T.G.; Klevtsova, R.F.; Uskov, E.M.; Platonov, V.E.; Karpov, V.M.; Fadeeva, V.P. Luminescence properties of complexes Ln(Phen)(C6F5COO)3 (Ln = Tb, Eu) and Ln(C6F5COO)3 · nH2O (Ln = Tb, n = 2; Ln = Eu, n = 1). Structures of the [Tb2(H2O)8(C6F5COO)6] complex and its isomer in the supramolecular compound [Tb2(H2O)8(C6F5COO)6] · 2C6F5COOH. *Russ. J. Coord. Chem.* **2009**, *35*, 798–806. [[CrossRef](#)]
37. Crosby, G.; Highland, R.; Truesdell, K. Spectroscopic properties of (nd)10 transition metal complexes. *Coord. Chem. Rev.* **1985**, *64*, 41–52. [[CrossRef](#)]
38. Shmelev, M.A.; Gogoleva, N.V.; Sidorov, A.A.; Nelyubina, Y.A.; Dolgushin, F.M.; Voronina, Y.K.; Kiskin, M.A.; Aleksandrov, G.G.; Varaksina, E.A.; Taydakov, I.V.; et al. Chemical assembling of heterometallic {Cd–M} (M=Li, Mg, Eu, Tb) molecules with 3,5-Di-tert-butylbenzoate bridges and N-donor ligands. *ChemistrySelect* **2020**, *5*, 8475–8482. [[CrossRef](#)]
39. Shmelev, M.A.; Voronina, Y.K.; Gogoleva, N.V.; Sidorov, A.A.; Kiskin, M.A.; Dolgushin, F.M.; Nelyubina, Y.V.; Aleksandrov, G.G.; Varaksina, E.A.; Taydakov, I.V.; et al. Influence of the steric properties of pyridine ligands on the structure of complexes containing the {LnCd2(bzo)7} fragment. *Russ. Chem. Bull.* **2020**, *69*, 1544–1560. [[CrossRef](#)]
40. Steemers, F.J.; Verboom, W.; Reinhoudt, D.N.; Van Der Tol, E.B.; Verhoeven, J.W. New Sensitizer-Modified Calix [4] arenes Enabling Near-UV Excitation of Complexed Luminescent Lanthanide Ions. *J. Am. Chem. Soc.* **1995**, *117*, 9408–9414. [[CrossRef](#)]
41. Werts, M.H.V.; Jukes, R.T.F.; Verhoeven, J.W. The emission spectrum and the radiative lifetime of Eu3+ in luminescent lanthanide complexes. *Phys. Chem. Chem. Phys.* **2002**, *4*, 1542–1548. [[CrossRef](#)]
42. Utochnikova, V.V.; Solodukhin, N.N.; Aslandukov, A.A.; Zaitsev, K.V.; Kalyakina, A.S.; Averin, A.A.; Ananyev, I.A.; Churakov, A.V.; Kuzmina, N.P. Luminescence enhancement by p-substituent variation. *Eur. J. Inorg. Chem.* **2017**, *1*, 107–114. [[CrossRef](#)]
43. Kahn, O. *Molecular Magnetism*; VCH Publishers Inc.: New York, NY, USA, 1993; p. 380.
44. Chilton, N.F.; Anderson, R.P.; Turner, L.D.; Soncini, A.; Murray, K.S. PHI: A powerful new program for the analysis of anisotropic monomeric and exchange-coupled polynuclear d- and f-block complexes. *J. Comput. Chem.* **2013**, *34*, 1164–1175. [[CrossRef](#)] [[PubMed](#)]

45. John, D.; Urland, W. Crystal structure and magnetic behaviour of the new gadolinium carboxylates Gd₂(ClF₂CCOO)₆(Hppy)₂, Gd₂(F₃CCOO)₆(Hppy)₂, Gd₂(F₂HCCOO)₆(Hppy)₂ and Gd₂(Cl₂HCCOO)₆(H₂O)₂(Hppy)₂. *Eur. J. Inorg. Chem.* **2006**, *2006*, 3503–3509. [[CrossRef](#)]
46. John, D.; Urland, W. Crystal Structure and Magnetic Behaviour of the New Gadolinium Complex Compound Gd₂(ClH₂CCOO)₆(bipy)₂. *Eur. J. Inorg. Chem.* **2005**, *2005*, 4486–4489. [[CrossRef](#)]
47. Gavrikov, A.; Koroteev, P.S.; Efimov, N.N.; Dobrokhotova, Z.V.; Ilyukhin, A.B.; Kostopoulos, A.; Ariciu, A.-M.; Novotortsev, V.M. Novel mononuclear and 1D-polymeric derivatives of lanthanides and (η⁶-benzoic acid)tricarbonylchromium: Synthesis, structure and magnetism. *Dalton Trans.* **2017**, *46*, 3369–3380. [[CrossRef](#)]
48. Mamontova, E.; Long, J.; Ferreira, R.A.S.; Botas, A.M.P.; Luneau, D.; Guari, Y.; Carlos, L.A.D.; Larionova, J. Magneto-Luminescence Correlation in the Textbook Dysprosium(III) Nitrate Single-Ion Magnet. *Magnetochemistry* **2016**, *2*, 41. [[CrossRef](#)]
49. Habib, F.; Lin, P.-H.; Long, J.; Korobkov, I.; Wernsdorfer, W.; Murugesu, M. The Use of Magnetic Dilution to Elucidate the Slow Magnetic Relaxation Effects of a Dy₂Single-Molecule Magnet. *J. Am. Chem. Soc.* **2011**, *133*, 8830–8833. [[CrossRef](#)]
50. Petrosyants, S.P.; Ilyukhin, A.B.; Efimov, N.N.; Gavrikov, A.; Novotortsev, V.M. Self-assembly and SMM properties of lanthanide cyanocobaltate chain complexes with terpyridine as blocking ligand. *Inorg. Chim. Acta* **2018**, *482*, 813–820. [[CrossRef](#)]
51. Bilyachenko, A.N.; Yalymov, A.I.; Korlyukov, A.A.; Long, J.; Larionova, J.; Guari, Y.; Zubavichus, Y.V.; Trigub, A.L.; Shubina, E.S.; Eremenko, I.L.; et al. Heterometallic Na₆ Co₃ Phenylsilsesquioxane Exhibiting Slow Dynamic Behavior in its Magnetization. *Chem. Eur. J.* **2015**, *21*, 18563–18565. [[CrossRef](#)]
52. Petrosyants, S.P.; Babeshkin, K.A.; Gavrikov, A.; Ilyukhin, A.B.; Belova, E.V.; Efimov, N.N. Towards comparative investigation of Er- and Yb-based SMMs: The effect of the coordination environment configuration on the magnetic relaxation in the series of heteroleptic thiocyanate complexes. *Dalton Trans.* **2019**, *48*, 12644–12655. [[CrossRef](#)] [[PubMed](#)]
53. Polyzou, C.D.; Koumoussi, E.S.; Lada, Z.G.; Raptopoulou, C.P.; Psycharis, V.; Rouzières, M.; Tsipis, A.C.; Mathonière, C.; Clérac, R.; Perlepes, S.P. “Switching on” the single-molecule magnet properties within a series of dinuclear cobalt(iii)–dysprosium(iii) 2-pyridyloximate complexes. *Dalton Trans.* **2017**, *46*, 14812–14825. [[CrossRef](#)] [[PubMed](#)]
54. Groom, C.R.; Bruno, I.J.; Lightfoot, M.P.; Ward, S.C. The Cambridge Structural Database. *Acta Crystallogr. B* **2016**, *72*, 171–179. [[CrossRef](#)] [[PubMed](#)]
55. Shmelev, M.A.; Kuznetsova, G.N.; Dolgushin, F.M.; Voronina, J.K.; Gogoleva, N.V.; Kiskin, M.A.; Ivanov, V.K.; Sidorov, A.A.; Eremenko, I.L. Influence of fluorinated aromatic fragments on the structure of cadmium and zinc carboxylate complexes by the example of pentafluorobenzoates and 2,3,4,5-tetrafluorobenzoates. *Russ. J. Coord. Chem.* **2021**, *47*, in press. [[CrossRef](#)]
56. Martínez-Pérez, M.J.; Cardona-Serra, S.; Schlegel, C.; Moro, F.; Alonso, P.J.; Prima-García, H.; Clemente-Juan, J.M.; Evangelisti, M.; Gaita-Ariño, A.; Sesé, J.; et al. Gd-Based Single-Ion Magnets with Tunable Magnetic Anisotropy: Molecular Design of Spin Qubits. *Phys. Rev. Lett.* **2012**, *108*, 247213. [[CrossRef](#)]
57. Arauzo, A.; Lazarescu, A.; Shova, S.; Bartolomé, E.; Cases, R.; Luzón, J.; Turta, C. Structural and magnetic properties of some lanthanide (Ln = Eu(iii), Gd(iii) and Nd(iii)) cyanoacetate polymers: Field-induced slow magnetic relaxation in the Gd and Nd substitutions. *Dalton Trans.* **2014**, *43*, 12342–12356. [[CrossRef](#)]
58. Holmberg, R.J.; Ho, L.T.A.; Ungur, L.; Korobkov, I.; Chibotaru, L.F.; Murugesu, M. Observation of unusual slow-relaxation of the magnetisation in a Gd-EDTA chelate. *Dalton Trans.* **2015**, *44*, 20321–20325. [[CrossRef](#)]
59. Yoshida, T.; Cosquer, G.; Izuogu, D.C.; Ohtsu, H.; Kawano, M.; Lan, Y.; Wernsdorfer, W.; Nojiri, H.; Breedlove, B.K.; Yamashita, M. Field-Induced Slow Magnetic Relaxation of Gd^{III} Complex with a Pt–Gd Heterometallic Bond. *Chem. Eur. J.* **2017**, *23*, 4551–4556. [[CrossRef](#)]
60. Handzlik, G.; Magott, M.; Arczyński, M.; Sheveleva, A.M.; Tuna, F.; Sarewicz, M.; Osyczka, A.; Rams, M.; Vieru, V.; Chibotaru, L.F.; et al. Magnetization Dynamics and Coherent Spin Manipulation of a Propeller Gd(III) Complex with the Smallest Helicene Ligand. *J. Phys. Chem. Lett.* **2020**, *11*, 1508–1515. [[CrossRef](#)]
61. Khalifaoui, O.; Beghidja, A.; Long, J.; Beghidja, C.; Guari, Y.; Larionova, J. Field-Induced Slow Relaxation in a Dinuclear Dysprosium(III) Complex Based on 3-Methoxycinnamic Acid. *Inorganics* **2018**, *6*, 35. [[CrossRef](#)]

62. Ishikawa, N.; Sugita, M.; Ishikawa, T.; Koshihara, A.S.-Y.; Kaizu, Y. Mononuclear Lanthanide Complexes with a Long Magnetization Relaxation Time at High Temperatures: A New Category of Magnets at the Single-Molecular Level. *J. Phys. Chem. B* **2004**, *108*, 11265–11271. [[CrossRef](#)]
63. Mandal, L.; Biswas, S.; Yamashita, M. Magnetic Behavior of Luminescent Dinuclear Dysprosium and Terbium Complexes Derived from Phenoxyacetic Acid and 2,2'-Bipyridine. *Magnetochemistry* **2019**, *5*, 56. [[CrossRef](#)]
64. SMART (control) and SAINT (integration) Software; Version 5.0; Bruker AXS Inc.: Madison, WI, USA, 1997.
65. Sheldrick, G.M. SADABS-2004/1, Program for Scaling and Correction of Area Detector Data; Göttingen University: Göttingen, Germany, 1997.
66. Dolomanov, O.V.; Bourhis, L.J.; Gildea, R.J.; Howard, J.A.K.; Puschmann, H. OLEX2: A complete structure solution, refinement and analysis program. *J. Appl. Crystallogr.* **2009**, *42*, 339–341. [[CrossRef](#)]
67. Sheldrick, G.A. Short history of ShelX. *Acta Cryst. Sect. A* **2007**, *64*, 112–122. [[CrossRef](#)]
68. Llunell, M.; Casanova, D.; Cirera, J.; Alemany, P.; Alvarez, S. SHAPE, Program. for the Stereochemical Analysis of Molecular Fragments by Means of Continuous Shape Measures and Associated Tools, version 2.1; University of Barcelona: Barcelona, Spain, 2013.

Publisher's Note: MDPI stays neutral with regard to jurisdictional claims in published maps and institutional affiliations.



© 2020 by the authors. Licensee MDPI, Basel, Switzerland. This article is an open access article distributed under the terms and conditions of the Creative Commons Attribution (CC BY) license (<http://creativecommons.org/licenses/by/4.0/>).